nature portfolio

Peer Review File

Triboelectric tactile sensor for pressure and temperature sensing in high-temperature applications

Corresponding Author: Professor Shuangxi Nie

Parts of this Peer Review File have been redacted as indicated to remove third-party material.

This file contains all reviewer reports in order by version, followed by all author rebuttals in order by version.

Attachments originally included by the reviewers as part of their assessment can be found at the end of this file.

Version 0:

Reviewer comments:

Reviewer #1

(Remarks to the Author)
Please see attached PDF.

Reviewer #2

(Remarks to the Author)
The author demonstrates a triboelectric tactile sensor that responds to pressure/temperature beyond the human tactile perception range in extreme environments. However, the devices are not innovative enough and the applications are not sufficiently sophisticated. Accordingly to the listed comments bellow, I do not think it satisfies the high standard of Nature Communications.
1. Flexible and self-powered temperature–pressure dual-parameter sensor with better performances has been studied and solved in better and superior ways (Nat. Commun. 2015, 6, 8356), and it's worth noting that the references related to the temperature-resistant flexible sensing for comparison (Fig. 3g) are not listed clearly in the manuscript.
2. According to proposed Wang's thermionic electron-emission model, the surface charge density slowly decreases with time at certain temperature (Fig .1c in Nat. Commun. 2020, 11, 399 and Fig. 1d in Adv. Mater. 2018, 30, 1706790.), leading to questionable quickly stabilization properties of T-TENG in this manuscript. However, with above mismatch, the authors did not further explore the equilibrium relationship of P-TENG output versus frequency under two opposite effects of thermionic electron emission and triboelectric initiation.
3. As multimodal sensing, the response speed obviously does not depend on one of the fastest sensors, and the response speed of T-TENG is not systematically considered.
4. Pressure sensing enhancements using surface micro processing but with higher sensitivity (>9.21 KPa-1) are common, the high sensitivity of the P-TENG is not theoretically sufficiently supported and the device structure is not an innovation.
5. CNF material is widely used as a temperature resistant material in high temperature resistant sensors (Cellu 2019, 26, 5291-5303; Pet. Sci. 2023）, and the principle of high temperature resistance realized only by high temperature resistant material is not innovative enough (Adv. Sci. 2020, 7, 2000258).
6. The T-TENG in the manuscript essentially operates as a single-electrode device, which is subject to severe electromagnetic interference, making it difficult to distinguish valid signals from interference in practical applications.
7. Experiments and all data are carried out and obtained in ideal experimental environments under standard conditions, and there is a lack of practical application demonstrations (e.g., videos) reflecting the core functionality of the dual-fusion sensor. Meanwhile, except for the temperature, other factors, like moisture, light and etc. would also affect the surface charge, so the output signal would be complicated in the real situation.

Reviewer #3

(Remarks to the Author)
The manuscript reports tactile sensor based on triboelectric generator. The sensor is capable of working at high temperature (200 deg celsius) and able to recognise objects of different shapes. The sensor has fast response and recovery time. The

manuscript lacks sufficient details required to reproduced the methods. Further, the results are not supported by explanations. I want to reject the manuscript and following comments can be considered:

1. The thickness of FEP and CNF is considered same in the COMSOL simulation which is not true. Further is it possible to consider surface roughness of nm range in the COMSOL simulations. If not what is the reliability of simulation.
2. What is the frequency used for response and recovery time. Is there any influence of frequency on the response and recovery time of the pressure sensor.
3. Why frequency has no influence on the signal of pressure sensor.
4. Please include at least six data points to confirm the linear relationship for the sensors.
5. "In the test at room temperature, the pressure response signal is unaffected by the temperature when the pressure exceeds 20 kPa". The reason for this is unclear.
6. What is the sensitivity, response and recovery time of the temperature sensor.
7. The experimental section is unclear and doesn't provide enough details on the methods used. It is not clear how the temperature measurements were performed.
8. "The temperature dependent cross coupling error of P TENG is less than 0.4%". Please elaborate this.
9. For fig. 4f what is the scenario when both temperature and pressure changes at same time.
10. Please demonstrate identification of objects by including non-symmetric objects.
11. The authors are advised to check throughly for the spelling and grammatical errors. Please also check figure numbers for example Line 150 includes figure 3f but its 2f.

Version 1:

Reviewer comments:

Reviewer #1

(Remarks to the Author)
Author addressed all the comments. It can be accepted for publication

Reviewer #2

(Remarks to the Author)
Although the authors have spent efforts in revising the manuscript. The main concern is the novelty. I still don't think this work reaches the high standard level of Nature Communications.

Reviewer #3

(Remarks to the Author)
The raised comments are addressed well.

Point-by-point Response to Reviewers' Comments

(Manuscript ID: NCOMMS-23-63750)

Reviewer #1 (Remarks to the Author):

The proposed TENG design is unique and appreciate the authors for multimodal analysis with single device. The authors can modify their manuscript by inclusion of the following.

Response: We sincerely thank the reviewer for carefully reviewing our work. Meanwhile, we are highly grateful for the reviewer's appreciation and generous comments on our work as "*The proposed TENG design is unique and appreciate the authors for multimodal analysis with single device.*", and the valuable feedback that we have used to improve the quality of our manuscript. We deeply apologize for the previously insufficient discussion in the experimental section, inappropriate expressions and tests in the article, as well as incomplete experiments. We very much agree with the reviewer's suggestion, and we have supplemented relevant tests and discussions in accordance with the feedback to enhance the comprehensiveness of the manuscript. We thank the reviewer again. The following is our point-by-point response to these comments.

1. How does the author confess that the CNF film have spherical bulge on it?

Response: Thank you for your insightful comments. We appreciate the opportunity to clarify and enhance the manuscript based on your suggestions. According to the suggestions, to confirm the presence of spherical protrusions on the surface of cellulose nanofiber (CNF) films, we employed two complementary characterization techniques, scanning electron microscopy (SEM) and atomic force microscopy (AFM), to observe the surface microstructure of the CNFs-2 film. The results revealed that the surface of the CNFs-2 film treated with low-temperature plasma technology exhibited irregular spherical-like structures, and some of these spheres were bonded together to form larger spherical-like structures (Supplementary Figs. 5, 6). To explain the formation mechanism of the spherical-like structures on the CNFs-2 film, the supplementary explanation of the surface spherical structure formation mechanism was provided (Supplementary Fig. 4). Furthermore, to more accurately express the experimental results, the structural schematic diagram was re-drew in the manuscript (Fig. 3b). In light of your feedback, we have included a more detailed description of these characterization techniques and their results in the revised manuscript. We believe these additions provide a comprehensive answer to your query. Details are as follows.

“The preparation flowchart of the temperature sensing material of T-TENG and the pressure sensing material of P-TENG is shown in Supplementary Fig. 4. High-purity cellulose raw material is purified from bagasse pulp board and then becomes nanofibrillated pulp through a high-pressure homogenization process. CNFs film material (thickness 63 ± 4 μm) was prepared by vacuum-assisted fiber self-assembly followed by hot pressing and drying. Subsequently, the cellulose sample prepared by water flow-assisted self-assembly was treated using a rapid low-temperature plasma discharge technique. Oxygen is introduced into the reaction chamber, and under applied energy, the gas is ionized into a uniform plasma. At the microscopic level, the oxygen plasma interacts with the cellulose, causing the breakdown of macromolecular chains at the interface. At the macroscopic level, the treated substrate surface produces an etching effect, forming CNFs films with micro-nano structures of varying sizes. Subsequently, the CNFs films without surface morphology and with surface morphology were reacted with 3-aminopropyltriethoxysilane (APTES) to obtain the temperature sensing material CNFs-1 film and the pressure sensing material CNFs-2 film, respectively.”

“The schematic diagram of P-TENG's amplification is shown in Fig. 3b. When pressure is applied, the FEP makes contact with the protruding spherical structures on the surface of CNFs-2. Due to the coupling effects of triboelectric charging and electrostatic induction, P-TENG can convert mechanical pressure into electrical signals.”

“Additionally, leveraging the intrinsic high-temperature resistance of cellulose, modifications were made chemically, along with the construction of a surface-like spherical structure (Supplementary Figs. 4-6).”

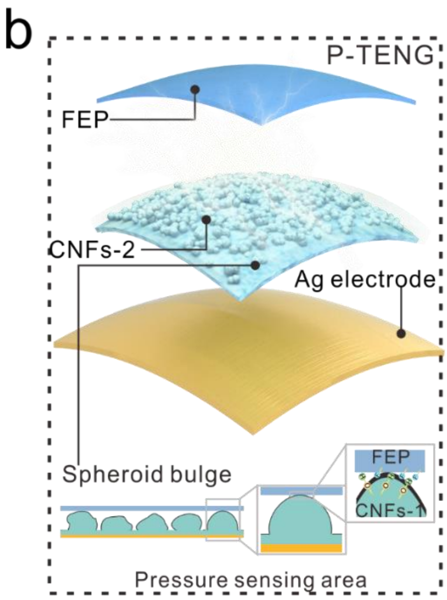

Fig. 3 | Pressure Sensing. b Structure of P-TENG.

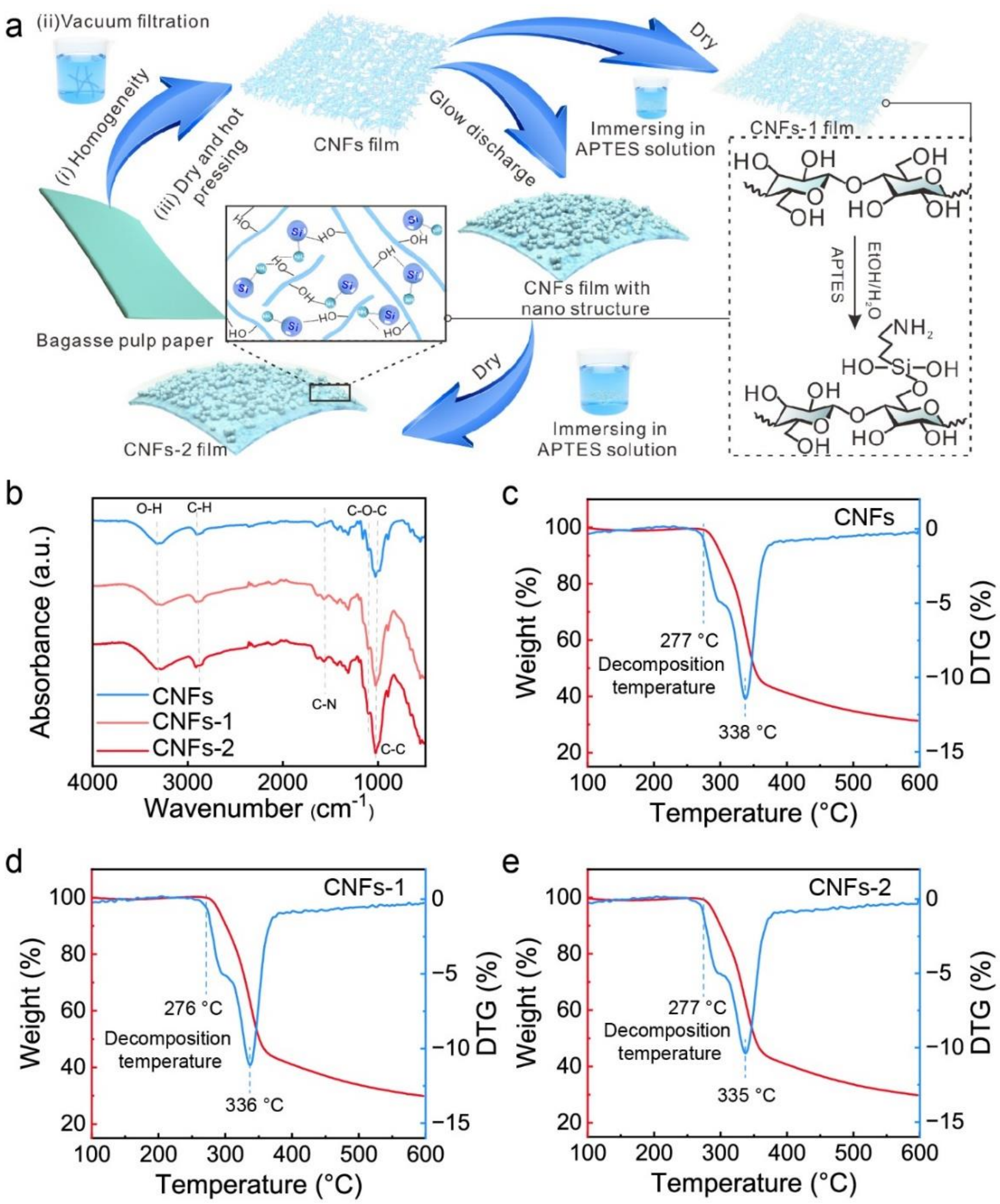

Supplementary Fig. 4 | Preparation of samples. **a** Schematic diagram of the preparation process of CNFs film, CNFs-1 film and CNFs-2 film (illustrated chemical process). **b** Fourier transform infrared spectral images of CNFs film, CNFs-1 film and CNFs-2 film. **c-e** Thermogravimetric analysis images of CNFs films, CNFs-1 film and CNFs-2 film, respectively.

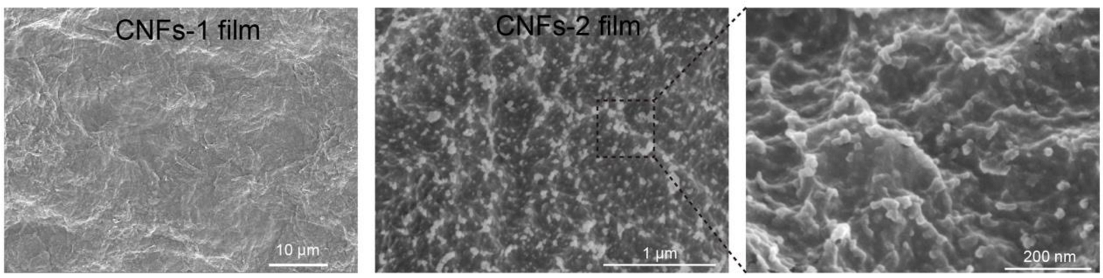

Supplementary Fig. 5 | Scanning electron microscopy (SEM) images of CNFs-1 film without surface microstructure and CNFs-2 film with surface structure.

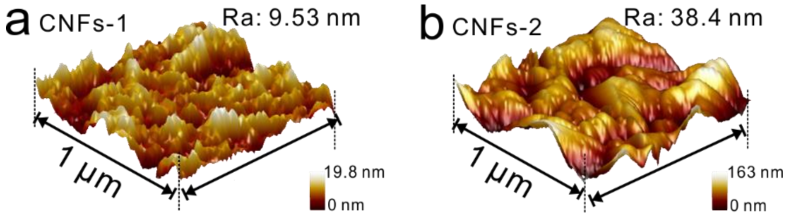

Supplementary Fig. 6 | Atomic Force microscope (AFM) images of CNFs-1 film without surface microstructure and CNFs-2 film with surface structure, with surface roughness (RA) of 9.53 nm and 38.4 nm, respectively.

2. Figure 2 a and 2 b needs more explanation for easy understanding.

Response: We greatly appreciate the reviewer's constructive suggestions to enhance the readability of our manuscript. To facilitate understanding for the readers, we have provided a detailed description of the preparation process of the dual-mode sensor and the structure of P-TENG (originally Fig. 2a, b, now revised to Fig, 3a, b). These specific modifications have been supplemented in the manuscript.

"The preparation process of the triboelectric sensor capable of responding to pressure/ temperature in extreme environments is illustrated in Fig. 3a and Supplementary Fig. 3. A structurally asymmetric dual-layer sensor by a two-step encapsulation strategy was designed to enable simultaneous sensing of pressure and temperature. To realize adaptive responses in extreme conditions, this work employs flexible, high-temperature-resistant silicone as an outer shell to facilitate rapid responsiveness to pressure stimuli (Fig. 3ai). Additionally, leveraging the intrinsic high-temperature resistance of cellulose37, modifications were made chemically, along with the construction of a surface-like spherical structure (Supplementary Figs. 4-6), to enhance the high-temperature triboelectric performance and sensing signals of cellulose materials (discussed in detail in Supplementary Fig. 7). The CNFs-1, with a silver electrode coating on its back, was affixed to the inner surface of the silicone shell at the top (small area side), while fluorinated ethylene propylene (FEP) was adhered and embedded to the middle position inside the shell, the T-TENG was prepared (Fig. 3aii-iv). Finally, a rough-surfaced CNFs-2, also coated with a silver electrode on its back, was affixed to the lower part of the silicone shell, sharing the FEP to construct P-TENG (Fig. 3av), thereby completing the dual-mode sensor (Fig. 3avi). The schematic diagram of P-TENG's amplification is shown in Fig. 3b. When pressure is applied, the FEP makes contact with the protruding spherical structures on the surface of CNFs-2. Due to the coupling effects of triboelectric charging and electrostatic induction, P-TENG can convert mechanical pressure into electrical signals."

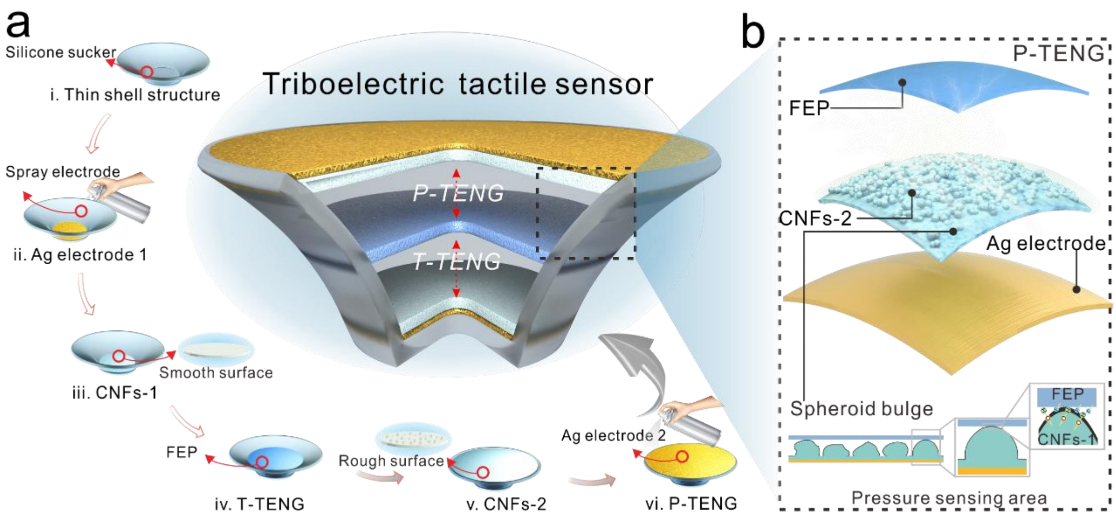

Fig. 3 | a Schematic diagram of the preparation process of the triboelectric sensor. **b** Structure of P-TENG.

3. The author should include real time photographs of fabricated device. (With the surface and cross-sectional SEM image of CNF 2 to verify its spherical roughness).

Response: We appreciate the reviewer's valuable feedback, particularly the suggestion for additional visual evidence to support our findings. Following the reviewer's recommendation, we have included real-time photographs of the device used to create the schematic in the supplementary information (Supplementary Fig. 3). By increasing the magnification in SEM observations, we have provided clearer surface images of the CNFs-2 film, revealing an irregular, rough, quasi-spherical morphology due to the randomness of the etching process (Supplementary Fig. 5). We apologize for not being able to obtain a good morphological image of the protruding surface roughness through cross-sectional observation, despite our best efforts. Additionally, we performed roughness tests using atomic force microscopy (Supplementary Fig. 6), which showed that the roughness of CNFs-1 and CNFs-2 were 9.53 nm and 38.4 nm, respectively, indirectly demonstrating the differences in surface structures. The relevant discussion has been supplemented, and all modifications are marked in red in the manuscript. The specific changes are as follows.

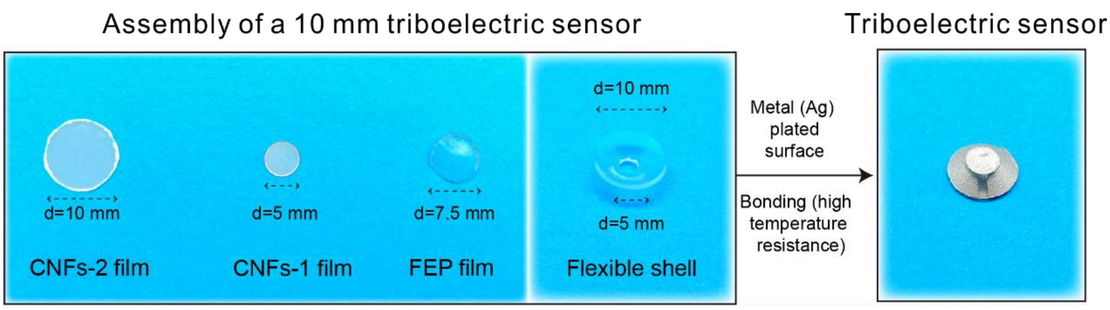

Supplementary Fig. 3 | Optical images of the triboelectric sensor components and assembly process.

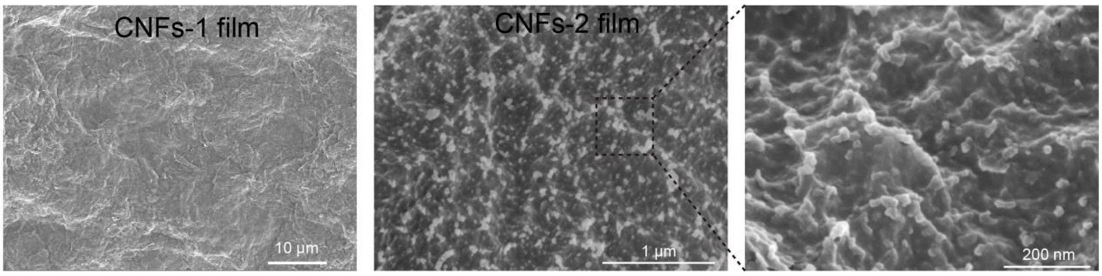

Supplementary Fig. 5 | Scanning electron microscopy (SEM) images of CNFs-1 film without surface microstructure and CNFs-2 film with surface structure.

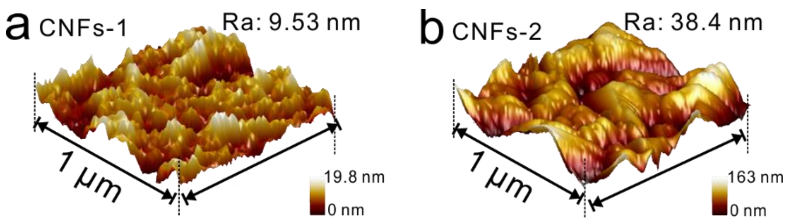

Supplementary Fig. 6 | Atomic Force microscope (AFM) images of CNFs-1 film without surface microstructure and CNFs-2 film with surface structure, with surface roughness (RA) of 9.53 nm and 38.4 nm, respectively.

4. How did the author perform electrical performance of the T-TENG and P-TENG? (Whether tested individually or multimodal setup itself).

Response: We appreciate your valuable feedback on our manuscript. We apologize for the unclear description of the experimental section in the manuscript, which failed to provide sufficient details about the methods used, making it difficult for readers to understand how the electrical properties of T-TENG and P-TENG were measured. To address your concerns, the detailed explanation of the electrical performance testing methods for T-TENG and P-TENG was provided. The electrical performance of TENG was measured using a Keithley 6514 electrometer. For standardized measurement of electrical output, a commercial linear mechanical motor applies a constant contact force, and the magnitude of the force is measured using a HYPX-601 instrument. The prepared T-TENG and P-TENG are attached to the fixed side of the HYPX-601 and a heating plate is secured on the linear motor side. The linear motor exerts pressure on the devices, inducing electron flow in the external circuit through the wires connected to CNFs-1 and CNFs-2 via contact electrification and electrostatic induction. The resulting electrical signals are measured by the electrometer and data are collected via a data acquisition card and displayed through computer software (Supplementary Fig. 16). According to the reviewer's comments, we have provided further detailed supplements on this testing process in the experimental section of the manuscript. The specific modifications are described as follows.

"The electrical performance of the dual TENGs was measured using a Keithley 6514 electrometer. For standard measurement of electrical output, a commercial linear mechanical motor is used to apply a constant contact force, with the magnitude of the applied force measured by a HYPX-601 instrument. The prepared T-TENG and P-TENG are respectively attached to the fixed side of the motor, and pressure is applied to the devices using a linear motor. The generated electrical signals are measured by the electrometer, then collected by a data acquisition card, and the final data is transferred to computer software for display. A schematic diagram of the experimental setup is shown in Supplementary Fig. 16."

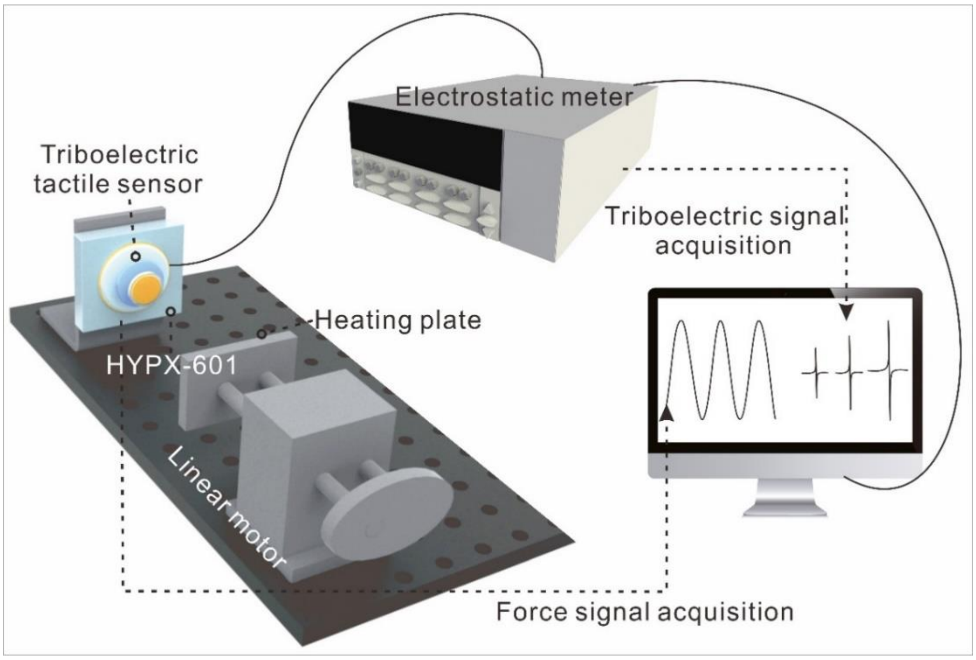

Supplementary Fig. 16 | Diagram of the electrical performance testing device.

5. Figure 3 d shows the pressure insensitivity of T-TENG, in a similar way does the PTENG is temperature insensitive?

Response: We greatly appreciate the reviewer's insightful questions and valuable suggestions, and we apologize for any shortcomings in the manuscript. It is worth noting that P-TENG, as a triboelectric pressure sensor, is inevitably influenced by temperature. In this study, we systematically investigated the effect of temperature on P-TENG, combining the temperature sensing signals from T-TENG to accurately decouple the sensing signals from P-TENG under dual stimuli of temperature and pressure. A comparison between the theoretical pressure sensing signals of P-TENG and those obtained from actual experiments reveals that the cross-coupling error in the pressure sensing signals due to temperature influence is less than 0.4%. This indicates the accuracy of P-TENG's pressure sensing signals even under high-temperature conditions. The details are as follows.

"In practical applications, multiple stimuli need to be detected simultaneously and independently. The signal interference between multiple coupled stimuli will affect the accuracy of the sensor, which requires the sensor to have low cross-interference and stable decoupling ability for the coupled signals (Fig. 5a). The signal interference of multimodal triboelectric sensors under fixed pressure and different temperatures was discussed (Fig. 5b). Compared with theoretical results (Supplementary Fig. 12), the cross-coupling errors of P-TENG and T-TENG due to temperature interference are less than 0.4% and 3.2%, respectively, indicating low cross-sensitivity between pressure and temperature. The low cross-sensitivity stems from the independence between the response mechanisms of the TENG signal to pressure and temperature stimulus (thermionic emission effect and contact area effect). The pressure response of P-TENG under different temperatures was further tested (Fig. 5c), and there was still a linear response between the pressure and Up of the triboelectric sensor at different temperatures. The linear relationship indicates that the relationship between Up and U_T and pressure and temperature can be related by the characteristic matrix M (Supplementary Note 4).

The feature matrix constructed from the linear dependence of the multimodal triboelectric sensor can be directly used for the stable decoupling of multiple signals. With known subcomponents of the feature matrix, unknown pressure (P) and temperature (T) can be obtained using the M and the values of U_P and U_T. Fig. 5d shows the corresponding relationship between pressure stimulation and temperature and U_P. Through feature matrix analysis, it's evident that components M_3 and M_4 are directly related to P-TENG, and M_3 has a mutual dependence with temperature (Fig. 5e). Fig. 5f and Supplementary Fig. 13 demonstrate the real-time response of the triboelectric sensor in complex scenarios with multiple coupled stimuli. Stable electrical signal responses can be achieved under conditions of individually varying temperature and pressure, as well as simultaneously varying pressure and temperature. Furthermore, to verify the sensor's potential in real complex scenarios, the stability of the signals in high humidity and strong UV irradiation environments was studied (Supplementary Fig. 14). It can be observed that the sensor's electrical response signals are stable, benefiting from the stability of the material and the encapsulation of the housing and electrodes. The demonstrations above verify the sensors' low cross-sensitivity to temperature and pressure signals, enabling the decoupling of dual stimuli through the feature matrix, and contributing to high-precision measurements in practical complex applications.”

[REDACTED]

Fig. 5 | Pressure-temperature decoupling and dual-modal sensing in a single triboelectric sensor. a Simultaneous extraction of two sensing parameters (pressure and temperature) by the matrix method. **b** Response signals of P-TENG and T-TENG at different temperatures under the pressure of 100 kPa. **c** Pressure parameters corresponding to the voltage signals of P-TENG at different temperatures. **d** Voltage signals of P-TENG when both pressure and temperature are applied. **e** Variation of the M_1M_3 and M_4 of the matrix under different temperatures. **f** Real-time response of the triboelectric sensor when subjected to temperature and pressure stimuli.

Finally, we sincerely appreciate the thoughtful and insightful comments. The manuscript has greatly benefited from these comments.

Reviewer #2 (Remarks to the Author):

The author demonstrates a triboelectric tactile sensor that responds to pressure/temperature beyond the human tactile perception range in extreme environments. However, the devices are not innovative enough and the applications are not sufficiently sophisticated. Accordingly to the listed comments bellow, I do not think it satisfies the high standard of Nature Communications.

Response: We sincerely appreciate your valuable feedback on our manuscript. We are deeply grateful for the time and effort you have dedicated to evaluating our work. We highly value and gladly accept your comments to enhance the novelty and advancements of our manuscript. Most importantly, we appreciate your candid opinions regarding the innovativeness and application complexity of our device, which have provided significant inspiration and guided us to reconsider the focus and imperfections of our manuscript. To address these concerns, we have reorganized the article, making point-by-point revisions and improvements to better showcase our main findings and contributions.

Regarding concerns about the device's lack of novelty, we have supplemented the revised manuscript with innovative elements in the sensor's material design, added the latest research progress on triboelectric sensors, and clearly articulated how our design pushes the advances of current technology. The novelty of our work lies not only in the fabrication of a dual-mode sensor but more importantly in demonstrating its potential for successful application in constructing temperature-pressure dual-response modules in extreme environments, exploring alternative and complementary pathways for sensing under such conditions. In response to the reviewer's concerns about applications, we have added experiments on the sensor's signal output under humidity and lighting conditions, as well as asymmetric object recognition experiments. This has also inspired our next phase of work, such as learning from mature solutions: the sensor can be connected to commercially available miniature signal acquisition and wireless transmission modules. These miniaturized, highly integrated devices can be matched with the sensor for more convenient detection. We also plan to integrate machine learning with circuits to achieve more complex object recognition, truly applying it to intelligent robots for special tasks. Moreover, we have supplemented contents not comprehensively considered in the original manuscript, including response time of temperature sensors, electromagnetic shielding, and testing signals in multifactorial scenarios. We are committed to solving these issues and believe the revised manuscript significantly improves in quality. We hope to receive the reviewers' approval and again sincerely thank you for your efforts, which are crucial in enhancing our manuscript's quality. Below are point-by-point responses to your comments.

1. Flexible and self-powered temperature–pressure dual-parameter sensor with better performances has been studied and solved in better and superior ways (Nat. Commun. 2015, 6, 8356), and it's worth noting that the references related to the temperature-resistant flexible sensing for comparison (Fig. 3g) are not listed clearly in the manuscript.

Response: We thank the reviewer for this insightful comment. The article mentioned by the reviewer (Nat. Commun. 2015, 6, 8356) has provided significant assistance to our work, for which we are deeply grateful and we have cited this in our discussion of the current state of research. We also sincerely apologize for the lack of specific references in Fig. 3g. We have supplemented this information in the manuscript, and we once again express our gratitude to the reviewer.

As the reviewer pointed out, Zhang et al. (Nat. Commun. 2015, 6, 8356) designed a flexible self-powered dual-parameter sensor for temperature and pressure using a microstructured framework supporting organic thermoelectric materials. This sensor effectively converts temperature and pressure stimuli into two independent electrical signals, enabling instantaneous sensing of temperature and pressure with precise temperature resolution and high pressure-sensing sensitivity. It provides an excellent and superior research solution for flexible self-powered temperature and pressure dual-parameter sensors. We believe that the ideas presented in this article are excellent, with a clear overall approach and outstanding innovation. It provides a comprehensive analysis and results for similar concepts, greatly assisting researchers in the field. Furthermore, we have drawn considerable inspiration from this work. Compared to Zhang et al.'s work, as described by the reviewer, our study presents the following innovations:

① Different scientific challenges were addressed: Zhang et al. addressed the simultaneous detection of temperature and pressure using a single device capable of accurate temperature sensing within the range of 0-60 °C under normal dynamic conditions, with a maximum test temperature of 130 °C. However, high temperatures and prolonged thermal contact cause temperature changes at the bottom electrode, impeding accurate measurements via thermoelectric mechanisms at higher temperatures. In contrast, we have tackled the simultaneous sensing of pressure and temperature at higher temperature (200 °C), which has not been achieved in previous works. Furthermore, we have proposed a novel approach for fabricating a temperature-pressure dual-sensing sensor based on the triboelectric generation principle in high-temperature environments, potentially driving technological innovation in related fields.

② Different performance focus: Indeed, Zhang et al. achieved precise temperature resolution (<0.1 K) and high pressure-sensing sensitivity (28.9 kPa^{-1}). Our work, however, demonstrates a signal output (20 V) that is over three orders of magnitude higher than related studies (0.3 mV), achieving a superior signal-to-noise ratio. In summary, each study has its own strengths and highlights, as shown in the comparison Table R1.

Table R1 | Systematic comparison between this study and Nat. Commun. 2015, 6, 8356

	Nat. Commun. 2015, 6, 8356	This study
Scientific problems	Sensitive temperature and pressure detection at the same time	Simultaneous sensing of pressure and temperature at high temperatures (200 °C)

Monitoring temperature range	0-130 °C	0-200 °C
Sensitivity	28.9 kPa^{-1}	9.21 kPa^{-1}
Signal to Noise Ratio	Low	High

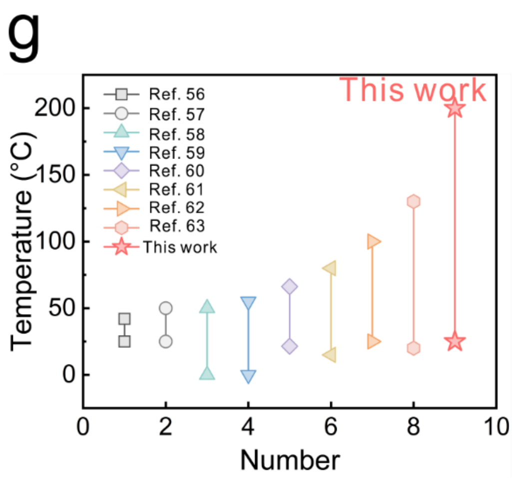

Fig. 4g (original Fig. 3g) | Comparison of T-TENG with other literature.

The additional references are as follows.

"[63] Zhang F, Zang Y, Huang D, Di C-a, Zhu DJNc. Flexible and self-powered temperature–pressure dual-parameter sensors using microstructure-frame-supported organic thermoelectric materials. 6, 8356 (2015)."

2. According to proposed Wang's thermionic electron-emission model, the surface charge density slowly decreases with time at certain temperature (Fig .1c in Nat. Commun. 2020, 11, 399 and Fig. 1d in Adv. Mater. 2018, 30, 1706790.), leading to questionable quickly stabilization properties of T-TENG in this manuscript. However, with above mismatch, the authors did not further explore the equilibrium relationship of P-TENG output versus frequency under two opposite effects of thermionic electron emission and triboelectric initiation.

Response: We sincerely appreciate your thorough examination of our manuscript and for highlighting critical aspects that require further clarification. Your insights regarding Wang's thermionic electron-emission model and its implications on the stabilization properties of T-TENG are invaluable.

As shown in Fig. 1c, d of the literature you mentioned, the phenomenon of surface charge density slowly decreasing over time in high-temperature environments is indeed particularly important when considering the rapid stability of T-TENG discussed in our manuscript. To address this issue, our current work mainly focuses on immediate operational output, but we acknowledge the lack of in-depth exploration of the longterm equilibrium dynamics involving electron thermionic emission and electrostatic initiation. We understand that these elements may significantly affect the performance and stability of P-TENG at different frequencies. In response, we supplemented experiments aimed at describing the equilibrium state of P-TENG output relative to frequency. This involves a detailed analysis of how thermionic emission and electrostatic initiation interact over time, which we believe will provide clearer insights into our thermionic emission and address the shortcomings you pointed out in your critique.

(1) We appreciate your efforts in highlighting these important works, which indeed contribute significantly to the context of our research. The articles by Lin et al. (Nat. Commun. 2020, 11, 399) and Cheng et al. (Adv. Mater. 2018, 30(15): 1706790) are crucial references for this research and have provided significant help, leading to citations within this paper ([46] and [7]). Lin et al. examined the decay of surface charges on solids after tribo-electrification with liquids under different thermal conditions by using the electron thermionic emission theory. They distinguished the contributions of electron transfer and ion transfer on charged surfaces. This research is highly significant for the study of TENG and electrical double-layer theory. Notably, Fig. 1d illustrates the exponential decay of surface charges affected by thermionic emission after liquid-solid contact, eventually stabilizing at high temperatures. Cheng et al. proposed an electron cloud potential well model based on an electron emission-dominated charge transfer mechanism through a TENG with a non-traditional inorganic-inorganic (Ti-SiO_2)-inorganic (Ti-Al_2O_3) structure. This model can be universally applied to explain all types of contact electrification in traditional materials. The research by Lin et al. and Cheng et al. explored charge transfer phenomena under high temperatures for both liquid-solid and solid-solid contact electrification mechanisms, forming the foundation of this study. We thank the reviewer again for their meticulous review.

“[46] Xu C, et al. Raising the working temperature of a triboelectric nanogenerator by quenching down electron thermionic emission in contact-electrification. Adv Mater 30, 1803968 (2018).

[7] Lin S, Xu L, Chi Wang A, Wang ZLJNc. Quantifying electron-transfer in liquid-solid contact electrification and the formation of electric double-layer. 11, 399 (2020) (Supplementary Information).”

(2) As the reviewer mentioned, "According to proposed Wang’s thermionic electron-emission model, the surface charge density slowly decreases with time at certain temperatures." This is quite accurate. In high-temperature environments, TENGs are inevitably affected by the thermionic electron emission effect, which causes the surface charge density to dissipate. As a result, the rise in temperature leads to the emission of triboelectric charges, significantly reducing the voltage signal and surface

charge density in the sensor studied, which is also the mechanism of T-TENG's temperature sensing. The thermionic emission mechanism of T-TENG follows the improved electron thermionic emission model proposed by Wang et al. (Adv. Mater. 2019, 31(17): 1808197), which is expressed as " $\sigma = \sigma_e e^{-at} + \sigma_p$". This model differs significantly from the general electron thermionic emission model ($\sigma = \sigma_e e^{-at}$). There are two different types of surface charges present on the surface of the triboelectric material. Apart from the shallow surface charges (σ_e) affected by temperature, which leads to the slow decline in surface charge density, there is another set of surface retained charges "σ_p" that are tightly bound to the material and less influenced by temperature. Moreover, in many existing high-temperature TENG studies (such as Nat. Commun. 2021, 12(1): 4782), the triboelectric materials used are often inorganic (such as Al and SiO_2) because high-performance positive polymers are not heat-resistant, and inorganic materials have weaker abilities to retain surface charges "σ_p". Consequently, we have developed cellulose-based triboelectric materials that are heat-resistant and have high retained surface charges "σ_p". To demonstrate the charge retention capability, we analyzed their molecular energy band structure, electron localization function, and carrier mobility to assess charge stability at high temperatures (Supplementary Note 3). Thanks to the design of cellulose triboelectric materials, the triboelectric sensor exhibits superior response times under temperature variations and has been validated in bimodal sensing, compared to other multi-modal sensors' temperature conversion response times (Fig. R1).

"**Supplementary Note 3 | Analysis of sensing principle for T-TENG**

According to the thermionic emission effect and extended the law of surface charge index decay at high temperature, Lin et.al (Adv. Mater. 31, 1808197 (2019)) further introduced the σ p term to describe the thermionic emission model,

$$J = \lambda A_0 T^2 e^{\frac{W}{kT}} \left[e^{\frac{\Delta w}{kT}} - 1 \right]$$

$$\sigma = e^{-at} \sigma_i$$

$$\sigma = e^{-at} \sigma_e + \sigma_p$$

Where J is the thermionic emission current density, λ is the material-specific correction factor, A_0 is the Richardson constant of free electrons, T is the temperature, W is the height of the potential barrier, k is the Boltzmann constant, ΔW is the change in the height of the potential barrier caused by the surface electric field, σ is the surface charge density, a is the decay coefficient, σ_i is the initial charge density, t is the dissipation time, σ_e is the triboelectric charge, σ_p is the "permanent" charge retained on the surface."

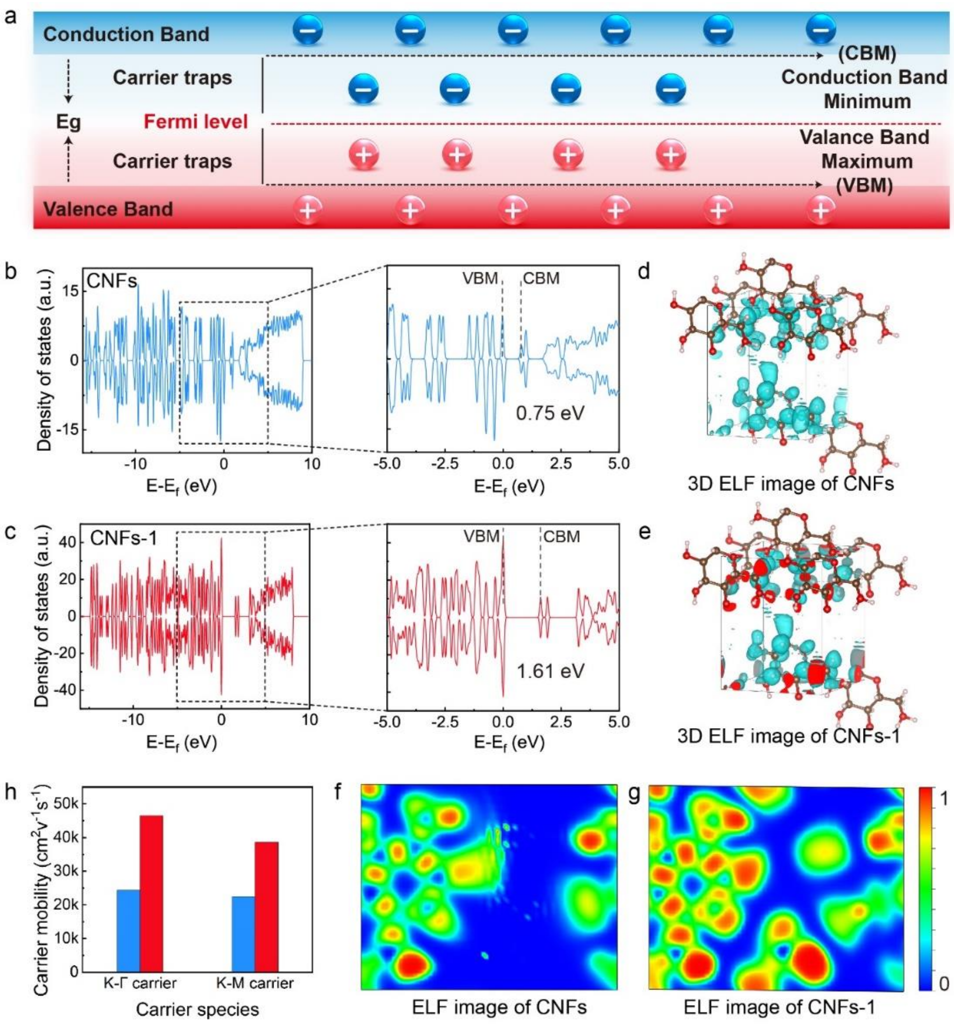

Supplementary Fig. 7 | Characterization of samples. a Schematic diagram of the electronic band structure of cellulose triboelectric materials. **b, c** Density of States (DOS) of the molecular structure of CNFs and CNFs-1. **d, e** Electron Localization Function (ELF) 3D images of the molecular structure of CNFs and CNFs-1 with isosurface of 0.61 e/Å3 (charge accumulation shown as cyan region). **f, g** ELF of the molecular structure of CNFs and CNFs-1. **h** Carrier mobility of the molecular structure of CNFs and CNFs-1 (the carrier type is electron-hole).

"Supplementary Fig. 7a presents a schematic diagram of the electronic band structure of cellulose triboelectric materials. The triboelectric charge generated by contact electrification is retained in the carrier traps of the band structure of the triboelectric material. The energy barrier and capture cross-section of the carrier traps confine the triboelectric charge to the electronic bandgap structure of the material. Density functional theory (DFT) analysis of the density of states (DOS) of CNFs films and the sensing material CNFs-1 reveals (Supplementary Fig. 7b, c) that the bandgap of CNFs films is only 0.75 eV, indicating that the carrier traps in the bandgap of CNFs films are closer to the band edges, requiring lower energy and resulting in weaker charge retention capability. The bandgap of CNFs-1 is significantly increased to 1.61 eV, and the bandgap of the triboelectric material in the charge retention phase is as high as 1.61 eV. The carrier traps for triboelectric charge are located far from the conduction band minimum and valence band maximum, respectively, which can better retain triboelectric charge and improve the sensor response signal.

To further investigate the redistribution of electrons in the molecular structure, the electron localization function (ELF) was calculated and topological analysis was performed. Supplementary Fig. 7d, e show the three-dimensional ELF visualization maps with an isosurface value of 0.61 e/Å3, respectively. The blue regions in the figures represent the electron distribution areas. Compared with CNFs, CNFs-1 has more blue distributions, indicating more electron distributions. The two-dimensional quantitative ELF images (Supplementary Fig. 7f, g) also show that the molecular structure of CNFs-1 has more electrons around it, indicating that in the charge retention phase, the transport process of triboelectric charge (carriers) makes it easier for triboelectric charge to bind with carrier traps, significantly improving triboelectric charge retention, which is more conducive to a higher sensor response signal in high-temperature environments.

To analyze the motion state of the charge in the sensing material, the carrier mobility is studied based on the variable situation theory proposed by Bardeen and Shockley, as shown in the equation:

$$\mu = \frac{eh^3C}{K_BTm^*m_dE_1^2}$$

Where e represents the elementary charge, $\hbar$ represents Planck's constant divided by 2π, K_B represents the Boltzmann constant, T represents the temperature set at 300 K. m* denotes the effective mass of electrons or holes, and the carrier mobility can be derived from the derivative of the electronic band structure using the following formula, as illustrated in Supplementary Fig. 7h. The results reveal that the CNFs film molecular structure exhibits a high carrier mobility (24298 $cm^2V^{-1}s^{-1}$), indicating the rapid motion of retained triboelectric charges within the band structure. Compared to CNFs, CNFs-1 exhibits further enhanced carrier mobility (46500 $cm^2V^{-1}s^{-1}$). DOS and ELF analyses demonstrate that CNFs-1 possesses a high triboelectric charge retention capability, leading to a more pronounced electrical response to stimuli. Additionally, CNFs-1 exhibits faster triboelectric charge motion. Under elevated temperatures, the rapidly moving triboelectric charges are susceptible to hot electron emission, resulting in a faster temperature change response for CNFs-1 in high-temperature environments.”

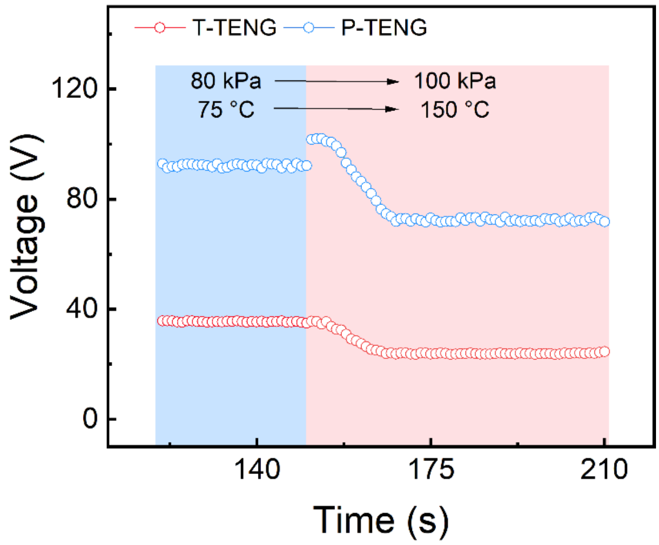

Supplementary Fig. 13 | The electrical signal in which pressure and temperature change simultaneously.

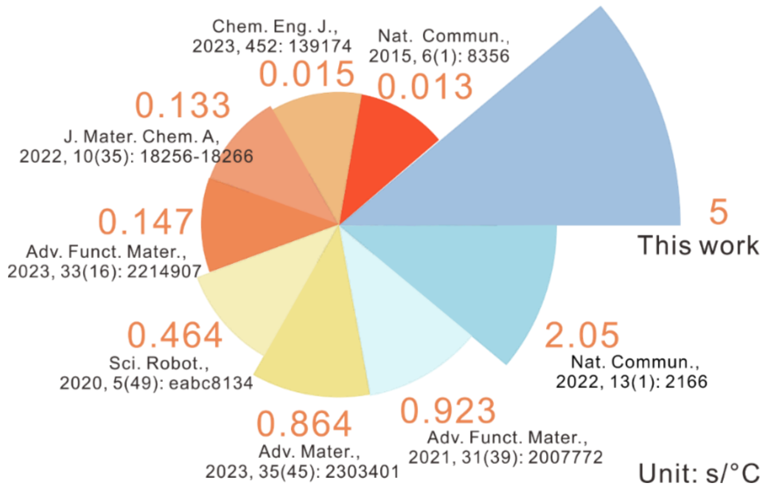

Fig. R1 | Comparison of temperature sensor response times.

(3) We strongly agree and acknowledge that we did not further explore the equilibrium relationship of P-TENG output versus frequency under two opposite effects of thermionic electron emission and triboelectric initiation. It is necessary to state that P-TENG, as a triboelectric pressure sensor, is affected by temperature, which is unavoidable. In this study, we systematically investigated the influence of temperature on P-TENG. By utilizing the temperature sensing signals provided by T-TENG, we accurately decoupled the sensing signals of P-TENG subjected to dual stimuli of temperature and pressure. By comparing the theoretical pressure sensing signals of P-TENG with those obtained in actual experiments, we found that the cross-coupling error of the pressure sensing signals under temperature influence is less than 0.4%. This indicates the accuracy of P-TENG's pressure sensing signals under high-temperature conditions. Additionally, we supplemented more detailed relationships between output and frequency. To clearly explain the specific impact of frequency on the response and

recovery times of the pressure sensor, we examined the response and recovery times at five different frequencies: 3 Hz, 2.5 Hz, 2 Hz, 1.5 Hz, and 1 Hz (Supplementary Fig. 10 and Table R2). In fact, frequency has a certain influence on the sensor's response and recovery times. The response time depends on the contact-separation time of the CNFs film material and FEP film material during pressure sensing. Faster frequencies can significantly enhance the response and recovery times of the sensor signals, with the fastest response and recovery times reaching 37 ms and 42 ms, respectively, under the rapid contact conditions of 3 Hz, while under the slow contact conditions of 1 Hz, response and recovery times can be maintained within 135 ms. Therefore, we have revised the manuscript's descriptions related to response and recovery times. The specific modifications are as follows.

"In practical applications, multiple stimuli need to be detected simultaneously and independently. The signal interference between multiple coupled stimuli will affect the accuracy of the sensor, which requires the sensor to have low cross-interference and stable decoupling ability for the coupled signals (Fig. 5a). The signal interference of multimodal triboelectric sensors under fixed pressure and different temperatures was discussed (Fig. 5b). Compared with theoretical results (Supplementary Fig. 12), the cross-coupling errors of P-TENG and T-TENG due to temperature interference are less than 0.4% and 3.2%, respectively, indicating low cross-sensitivity between pressure and temperature. The low cross-sensitivity stems from the independence between the response mechanisms of the TENG signal to pressure and temperature stimulus (thermionic emission effect and contact area effect). The pressure response of P-TENG under different temperatures was further tested (Fig. 5c), and there was still a linear response between the pressure and Up of the triboelectric sensor at different temperatures. The linear relationship indicates that the relationship between Up and U_T and pressure and temperature can be related by the characteristic matrix M (Supplementary Note 4).

The feature matrix constructed from the linear dependence of the multimodal triboelectric sensor can be directly used for the stable decoupling of multiple signals. With known subcomponents of the feature matrix, unknown pressure (P) and temperature (T) can be obtained using the M and the values of U_P and U_T. Fig. 5d shows the corresponding relationship between pressure stimulation and temperature and U_P. Through feature matrix analysis, it's evident that components M_3 and M_4 are directly related to P-TENG, and M_3 has a mutual dependence with temperature (Fig. 5e)."

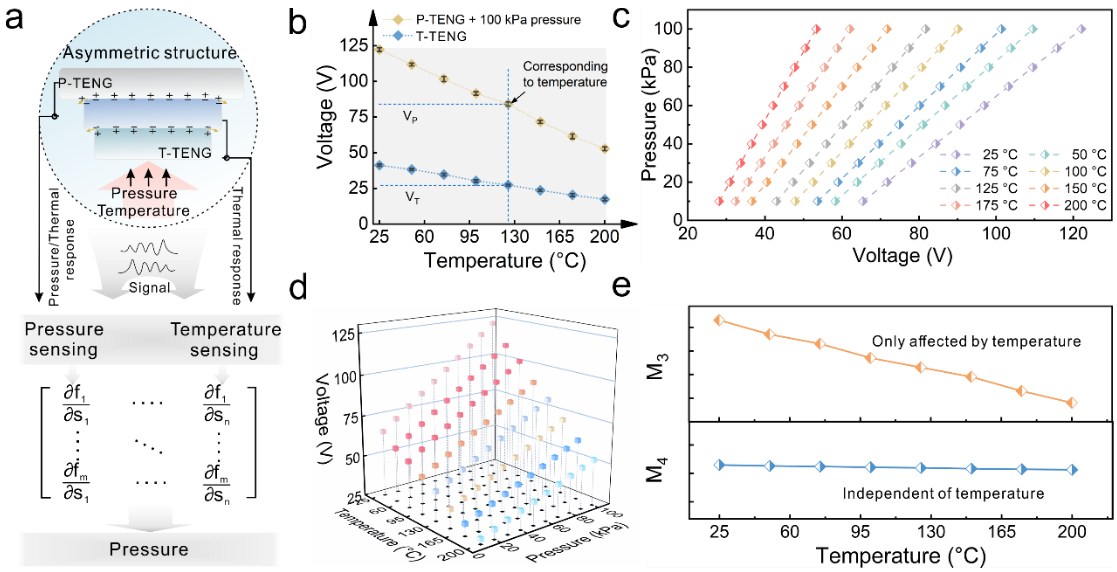

Fig. 5 | Pressure-temperature decoupling and dual-modal sensing in a single triboelectric sensor. a Simultaneous extraction of two sensing parameters (pressure and temperature) by the matrix method. **b** Response signals of P-TENG and T-TENG at different temperatures under the pressure of 100 kPa. **c** Pressure parameters corresponding to the voltage signals of P-TENG at different temperatures. **d** Voltage signals of P-TENG when both pressure and temperature are applied. **e** Variation of the M_1M_3 and M_4 of the matrix under different temperatures.

"When pressure was applied to P-TENG at 2 Hz, the response times to stress compression and recovery were 70 ms and 58 ms, respectively (Fig. 3e), and the higher response time is maintained at different frequencies (Supplementary Fig. 10), much faster than the human response time to tactile stimuli (139 ms)."

Table R2 | Response and recovery times of the pressure sensor at 3 Hz, 2.5 Hz, 2 Hz, 1.5 Hz and 1 Hz.

Frequency	3 Hz	2.5 Hz	2 Hz	1.5 Hz	1 Hz
Response time (ms)	37	50	70	104	134
Recovery time (ms)	42	52	58	96	131

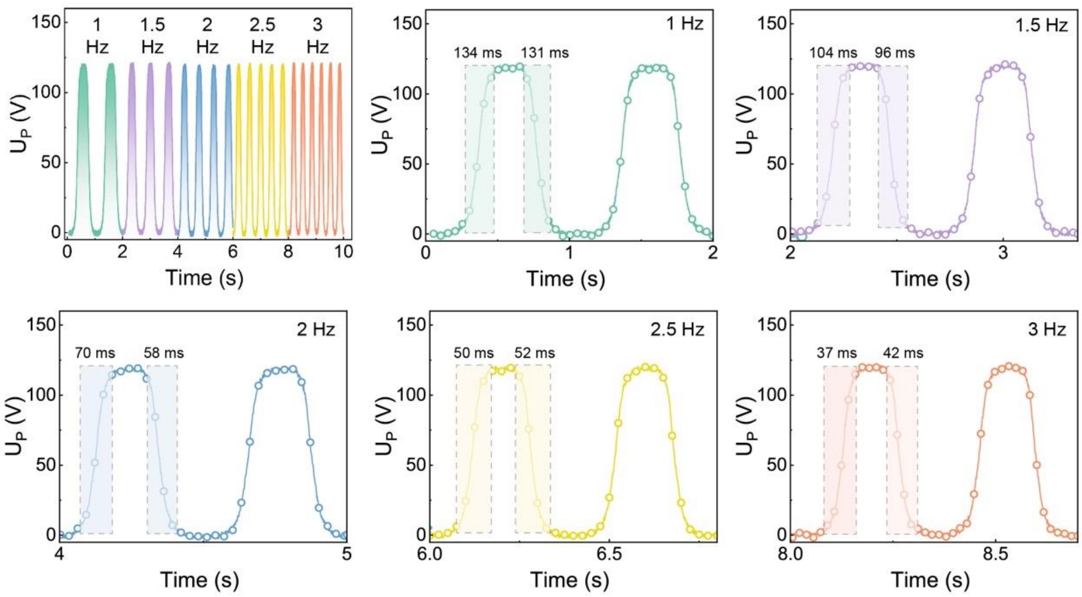

Supplementary Fig. 10 | Electrical signal and response time of the pressure sensor at 3 Hz, 2.5 Hz, 2 Hz, 1.5 Hz and 1 Hz.

3. As multimodal sensing, the response speed obviously does not depend on one of the fastest sensors, and the response speed of T-TENG is not systematically considered.

Response: We sincerely appreciate your valuable feedback and review of our manuscript. Your insights are crucial for improving the clarity and rigor of our work. Regarding the issue of response time in multimodal sensing systems that you mentioned, we acknowledge that we did not adequately consider the response time of T-TENG in the initial manuscript. While quick response is often an advantage of multimodal systems, it is indeed important to consider response time comprehensively and not just rely on the most sensitive sensor. To address this, we have added an experiment testing the response time of the temperature sensor. At an operating frequency of 2 Hz, the response time and recovery time of 67 ms and 63 ms, respectively, which are close to those of the P-TENG (Supplementary Fig. 11). The detailed modifications are as follows.

"Fig. 4c shows the continuous response of output voltage to temperature, exhibiting distinguishable and stable signals. At 2 Hz, the response times are 67 ms and 63 ms, respectively, which are close to those of the P-TENG (Supplementary Fig. 11). The linear response coefficient of sensitivity for the T-TENG is 0.996, indicating a good linear relationship between the electrical signal and temperature."

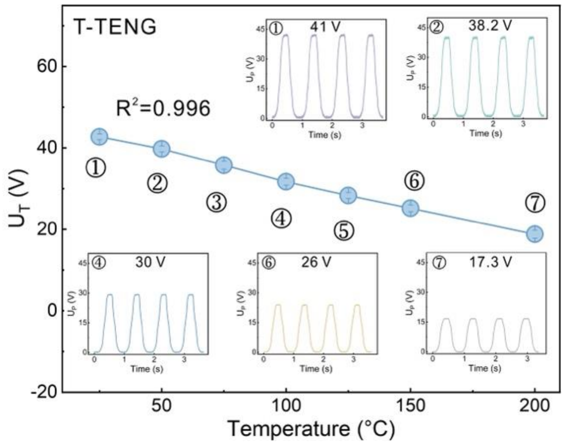

Fig. 3 | Temperature sensing. c Temperature sensing data.

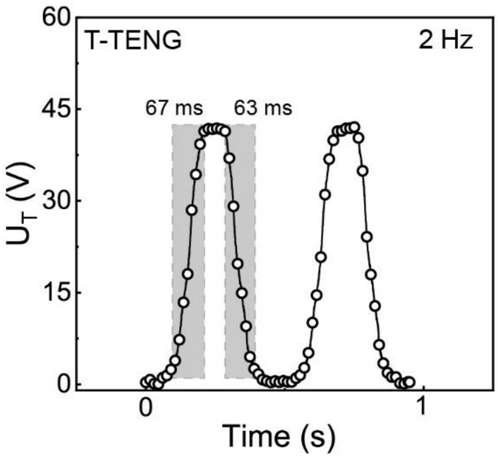

Supplementary Fig. 11 | Response and recovery time of T-TENG.

4. Pressure sensing enhancements using surface micro processing but with higher sensitivity (>9.21 KPa^{-1}) are common, the high sensitivity of the P-TENG is not theoretically sufficiently supported and the device structure is not an innovation.

Response: We sincerely appreciate your thorough review and insightful comments on our manuscript. Your feedback is invaluable in refining our work, and we are grateful for the opportunity to address your concerns regarding the theoretical support for our P-TENG's sensitivity and its structural innovation.

(1) We acknowledge that surface micro processing is often employed to enhance sensitivity, and respect the opinion that the work offers limited device innovation. Our research aims to explore the successful application of dual-responsive building blocks for temperature and pressure in extreme environments. The uniqueness of our P-TENG lies in its integration of high-temperature sensing and pressure sensing capabilities, enabling tactile sensing at high temperatures, which is uncommon in existing designs. For instance, the asymmetric structure adapts well to the installation on robotic fingers (Fig. 2a-c) and effectively identifies signals from grasped objects, significantly enhancing the practical application of multimodal tactile sensors.

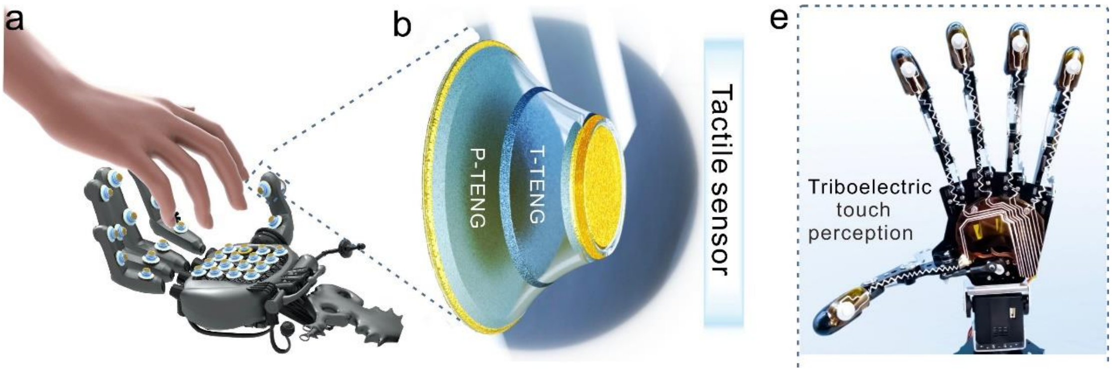

Fig. 2 | **a** Schematic illustration of the triboelectric sensor for human-machine interaction. **b** Detailed structure of the sensor. **c** Optical image of the triboelectric sensor integrated on robotic hand with stretchable electrodes.

(2) As the reviewer noted, pressure sensing enhancements using surface micro processing but with higher sensitivity (>9.21 kPa^{-1}) are common. However, we sincerely beg that you consider the comprehensive performance of our dual-modal sensor, the primary focus of this study is not on improving pressure sensor sensitivity. But in the realm of dual-modal tactile sensors, pressure sensing sensitivity (>9.21 kPa^{-1}) still offers certain advantages over existing research. In support of this, we have provided a comparative table (Supplementary Table 2) of triboelectric pressure sensor sensitivities from the recent years. Moreover, we have analyzed the temperature sensing capabilities of multimodal sensors in recent studies. Most research remains within the skin-perceivable temperature range (0-50 °C), limited by material, sensing mechanisms, and structural design constraints (Supplementary Table 1). In contrast, our study's dual-modal sensor broadens the temperature sensing range of multimodal sensors to 200 °C. This research offers new insights and opportunities for advancing multimodal sensing technology and robotic tactile sensing.

Supplementary Table 2 | The P-TENG sensitivity is compared with the reported pressure sensitivity of triboelectric sensors.

Sensing strategy	Pressure range (kPa)	Sensitivity	Reference
P-TENG	0-9.21	10.3 kPa^{-1}	***This work***
Fingertip inspired Liesegang patterns	0-35	1.5 V kPa^{-1}	*Adv. Mater. 2023, 2300593*
Micro/nanostructures on both tribo-materials	0-3.3 3.4-13	0.31 kPa^{-1} 0.01 kPa^{-1}	*Adv. Funct. Mater. 2024, 2402233*
Hierarchically porous structure	5.31-13.81	0.4023 kPa^{-1}	*Nano Energy 2024, 121, 109252.*
Knitted double-ribbed structure	2-8	0.28 V kPa^{-1}	*Adv. Funct. Mater. 2023, 33, 2303562*
Multi-peak microstructures and stripe-like convex structures	0-10	0.98 V kPa^{-1}	*Adv. Funct. Mater. 2024, 2401913*
Electrospun Ordered Hierarchical Microhump Arrays	3-15.63	3.7 V kPa^{-1}	*Adv. Funct. Mater. 2023, 33, 2301589*

Core-shell yarn structures	1.95-3.13 3.2-4.61	1.33 V kPa^{-1} 0.32 V kPa^{-1}	*ACS Appl. Mater 2020, 12, 19965*
Endoplasmic reticulum rGO microstructure	0-10	6.28 kPa^{-1}	*Chemical Engineering Journal 2022, 445, 136821*

Supplementary Table 1 | Comparison of the temperature detection range of this work with reported multimodal sensors.

Multimodal sensing	Sensing mechanism	Temperature range (°C)	Reference
Pressure/temperature	Stress-optic/thermo-optic	26-35	*ACS Appl. Mater.*, 2023, 53264-53272
Pressure/temperature	Piezocapacitive/ thermoresistive	30-45	*Nat. Commun.* 2018, 9, 2458
Pressure/temperature	Piezo-tribophotonic/ thermoresistive	30-50	*ACS Nano* 2022, 16, 2789
Pressure/temperature	Reverse electrowetting/ thermogalvanic	5-31	*Angew. Chem. Int. Ed.* 2016, 55, 15864
Strain/temperature	Transmittance/ thermoresistive	25-42	*Small* 2023, 2301868
Pressure/temperature	Piezoresistive/thermoresistive	25-50	*Adv. Funct. Mater.* 2022, 32, 2107570
Strain/temperature /pressure	Mechanochromic/thermoresistive /triboelectric	0-50	*Adv. Funct. Mater.* 2022, 32, 2208362
Pressure/temperature	Triboelectric	25-200	This work

(3) We acknowledge that the original manuscript did not sufficiently elucidate the theoretical foundation for the achieved sensitivity. To address this limitation, we have expanded the discussion in the revised manuscript, providing a more comprehensive theoretical analysis. Specifically, the sensitivity commonly observed in triboelectric sensor depends on the magnitude of the electrical signal responsive to applied pressure. Detailed theoretical support has been added to the revised supplementary information.

"**Supplementary Note 2 |** Theoretical analysis of pressure and voltage sensing signal (J. Mater. Chem. A, 2021, 9(36): 20100-20130)

Usually, under pressure P, the output voltage V_p of a TENG equals the open-circuit voltage V_{OC} in that state, which can be expressed by formula:

$$V_p = \frac{\sigma_0 d_p}{\varepsilon_0}$$

Where ε_0 is the vacuum permittivity constant, and σ_0 is the triboelectric charge density, considered constant. Assume the initial gap distance is d_0 with a change Δd, and d_p is the distance under pressure P. The gap distance and open-circuit voltage under pressure P can be calculated as follows:

$$d_p = d_0 - \frac{d_0}{Y} P$$

$$V_p = \frac{\sigma_0}{\varepsilon_0}\left(d_0 - \frac{d_0}{Y} P\right)$$

Where Young's modulus Y, the initial distance of the gap layer d_0, triboelectric charge density σ_0 , and permittivity constant ε_0 can be considered constants. The open-circuit voltage V_p is expected to have a direct linear relationship with the external pressure P, making it a reliable parameter for measuring the pressure applied to the sensor. The sensitivity calculation equation for the triboelectric pressure sensor is as follows:

$$S = d(\Delta V / V_s)/dP$$

Where ΔV is the relative change in output voltage, and V_s is the minimum detectable electrical signal. Different voltage increases lead to different sensitivities. Hence, the larger the voltage signal, the higher the sensitivity (Adv. Mater., 2022, 34(29): 2203073; Adv. Funct. Mater., 2019, 29(41): 1806379)."

5. CNF material is widely used as a temperature resistant material in high temperature resistant sensors (Cellu 2019, 26, 5291-5303; Pet. Sci. 2023), and the principle of high temperature resistance realized only by high temperature resistant material is not innovative enough (Adv. Sci. 2020, 7, 2000258).

Response: We sincerely appreciate the reviewers' inspiring comments and their efforts to improve our manuscript. We apologize for the previous inadequate description of the materials, which failed to convey the novelty and significance of our work. Your feedback made us aware of the shortcomings in the original manuscript regarding material presentation, and we have emphasized the advancements and innovative aspects of our high-temperature sensing materials in the revised version.

Thank you for providing information on related works, we have added these articles as references ([19] and [37]). After carefully reading and analyzing the literature you mentioned, we can highlight our work's novel aspects compared to existing studies. Our research explores the intrinsic high-temperature resistance of cellulose and its untapped potential in triboelectric sensing technologies. For instance, we have " investigating modified cellulose materials' ability to reduce charge carrier mobility via density functional theory calculations, and proposed and thoroughly studied its charge retention capability in high-temperature environments, as well as preliminary dual-modal sensing under high-temperature conditions." These represent novel research directions that have yet to be fully explored.

(1) The article described by the reviewer (Cellu 2019, 26, 5291-5303) utilizes functionalized CNF as a chemical cross-linking agent to prepare high-temperature resistant cellulose nanofiber/polyvinyl alcohol hydrogels. These hydrogels exhibit thermal stability during high-temperature sterilization (121 °C), providing an excellent approach for constructing materials for extreme environments. We apologize for not finding the literature (Pet. Sci. 2023). Another article (Adv. Sci. 2020, 7, 2000258) innovatively designs a pressure sensor that operates normally in high-temperature harsh conditions based on the high-temperature resistance of ceramic nanofibers. This work inspires future sensor material selection for extreme environments and promotes the practical application of wearable sensors under both routine and extreme conditions. In contrast, our work demonstrates the integration of temperature-pressure multisensory inputs and explores the operating mechanisms of the device, thereby potentially inspiring the design of next-generation multi-responsive electronics for extreme environments.

To visually showcase the differences, Table R3 summarizes the key points of the referenced literature compared to our study. We greatly appreciate the reviewers giving us the opportunity to illustrate the importance of this research and sincerely hope our response meets your approval.

Table R3 | Systematic comparison between this study and Cellu 2019, 26, 5291-5303, Adv. Sci. 2020, 7, 2000258

Frequency	Cellulose 2019, 26, 5291-5303	Adv. Sci. 2020, 7, 2000258	This work
Scientific problems	High-temperature resistant cellulose nanofibers/polyvinyl alcohol hydrogels	Pressure sensor for normal operation in high temperature and harsh environment	Simultaneous sensing of pressure and temperature at high temperatures (200 °C)
Sensing mode	No	Pressure	Pressure/Temperature
Sensitivity	No	4.4 kPa^{-1}	9.21 kPa^{-1}
Signal to Noise Ratio	No	Low	High

“[19] Fu, M. et al. A highly sensitive, reliable, and high‐temperature‐resistant flexible pressure sensor based on ceramic nanofibers. 7, 2000258 (2020)

[37] Zhu L, Liu Y, Jiang Z, et al. Highly temperature resistant cellulose nanofiber/polyvinyl alcohol hydrogel using aldehyde cellulose nanofiber as cross-linker[J]. Cellulose, 2019, 26: 5291-5303.”

(2) To comprehensively demonstrate the distinctions between the CNFs material utilized in this study and conventional CNFs, we have provided an in-depth presentation of the preparation methods, chemical characteristics, and high-temperature resistance properties of our CNFs material. The sensing materials (CNFs-1 and CNFs-2 films) were fabricated based on high-temperature resistant cellulose nanofibers. Detailed experimental procedures and characterization techniques are elucidated in the supplementary materials (Supplementary Figs. 4-6).

“The preparation flowchart of the temperature sensing material of T-TENG and the pressure sensing material of P-TENG is shown in Supplementary Fig. 4. High-purity cellulose raw material is purified from bagasse pulp board and then becomes nanofibrillated pulp through a high-pressure homogenization process. CNFs film material (thickness 63 ± 4 μm) was prepared by vacuum-assisted fiber self-assembly followed by hot pressing and drying. Subsequently, the cellulose sample prepared by water flow-assisted self-assembly was treated using a rapid low-temperature plasma discharge technique. Oxygen is introduced into the reaction chamber, and under applied energy, the gas is ionized into a uniform plasma. At the microscopic level, the oxygen plasma interacts with the cellulose, causing the breakdown of macromolecular chains at the interface. At the macroscopic level, the treated substrate surface produces an etching effect, forming CNFs films with micro-nano structures of varying sizes. Subsequently, the CNFs films without surface morphology and with surface morphology were reacted with 3-aminopropyltriethoxysilane (APTES) to obtain the temperature sensing material CNFs-1 film and the pressure sensing material CNFs-2 film, respectively.”

“Additionally, leveraging the intrinsic high-temperature resistance of cellulose, modifications were made chemically, along with the construction of a surface-like spherical structure (Supplementary Figs. 4-6).”

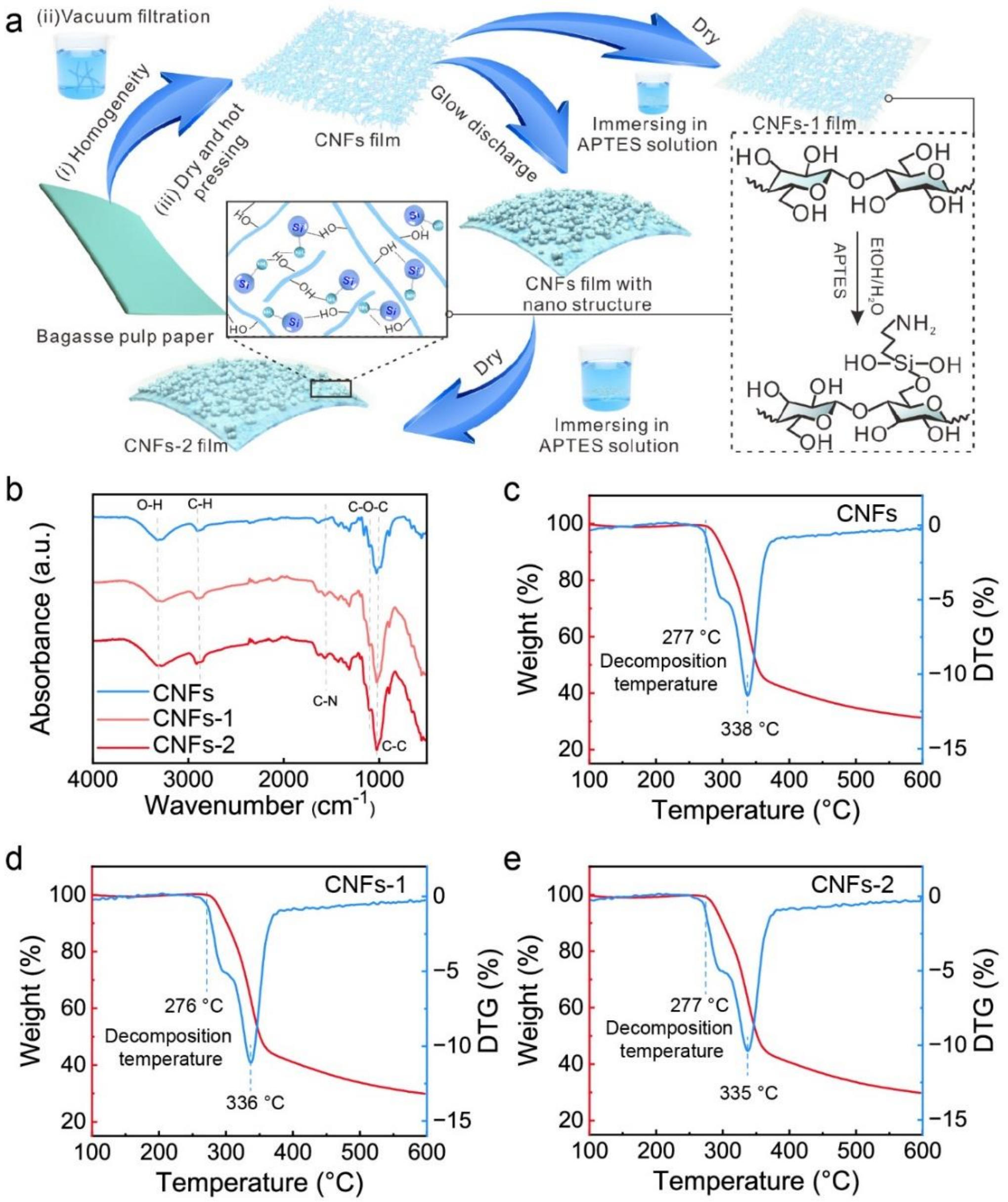

Supplementary Fig. 4 | Preparation of samples. **a** Schematic diagram of the preparation process of CNFs film, CNFs-1 film and CNFs-2 film (illustrated chemical process). **b** Fourier transform infrared spectral images of CNFs film, CNFs-1 film and CNFs-2 film. **c-e** Thermogravimetric analysis images of CNFs films, CNFs-1 film and CNFs-2 film, respectively.

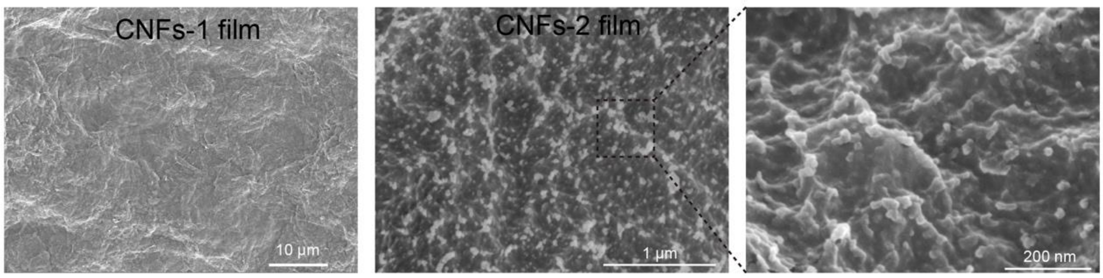

Supplementary Fig. 5 | Scanning electron microscopy (SEM) images of CNFs-1 film without surface microstructure and CNFs-2 film with surface structure.

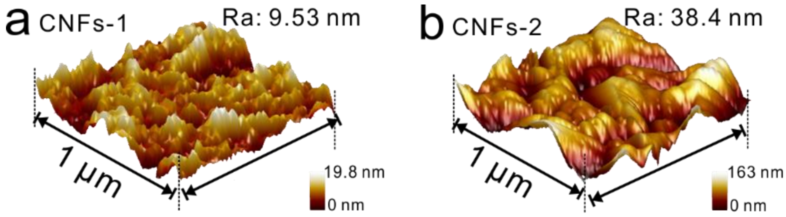

Supplementary Fig. 6 | Atomic Force microscope (AFM) images of CNFs-1 film without surface microstructure and CNFs-2 film with surface structure, with surface roughness (RA) of 9.53 nm and 38.4 nm, respectively.

(3) We are grateful for your suggestions, which have prompted us to conduct a more in-depth supplementary investigation into the crucial characterization of electrical properties. The extended analysis includes the density of states (DOS), electron localization function (ELF), and carrier mobility, elucidating the value and innovativeness of cellulose materials for high-temperature triboelectric sensor applications.

The wide bandgap indicated by the DOS highlights cellulose's potential as an effective electronic insulator, thereby maximizing charge retention capacity. This characteristic is particularly important for sensors requiring stable charge storage and reduced leakage current. The ELF provides a graphical representation of electron distribution and localization, which is critical for understanding how electrons are confined within specific molecular groups in the cellulose materials. Furthermore, examining carrier mobility has clarified the reasons for charge retention at high temperatures. Our comprehensive analysis of these properties underscores cellulose's innovative potential in advancing cutting-edge sensor technology development.

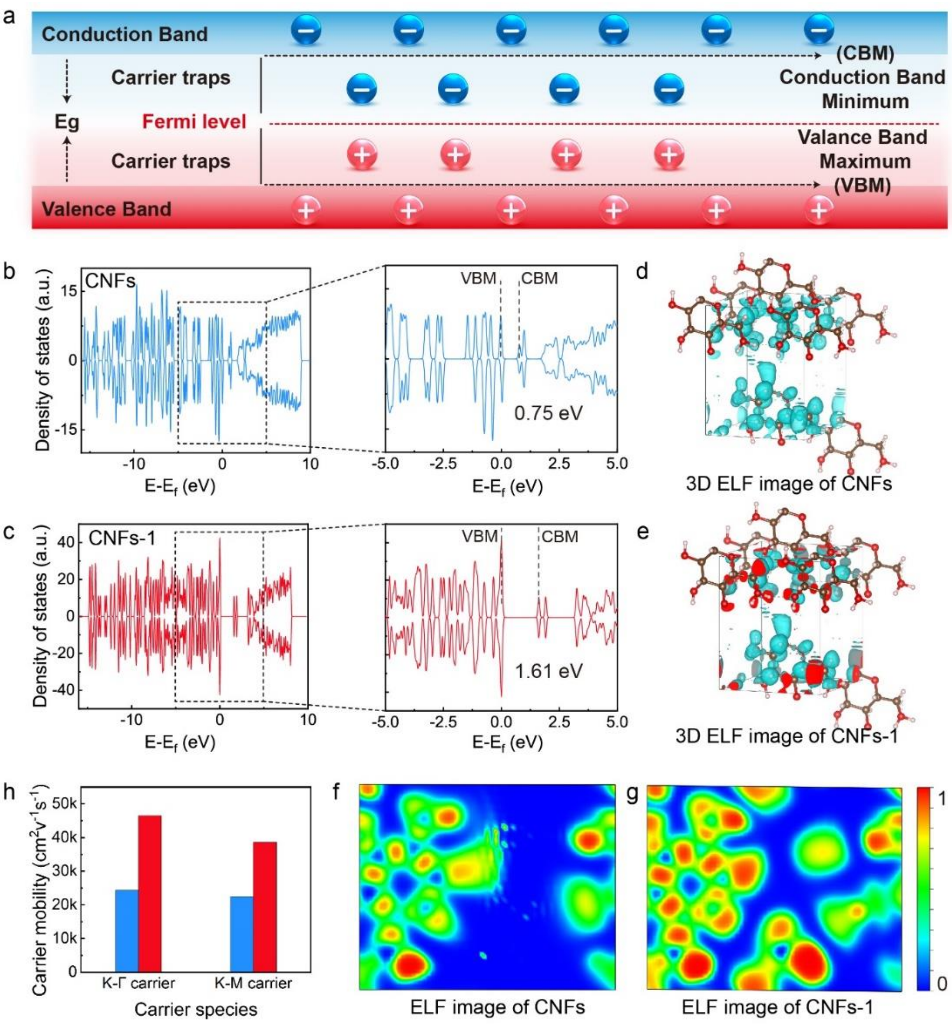

Supplementary Fig. 7 | Characterization of samples. a Schematic diagram of the electronic band structure of cellulose triboelectric materials. **b, c** Density of States (DOS) of the molecular structure of CNFs and CNFs-1. **d, e** Electron Localization Function (ELF) 3D images of the molecular structure of CNFs and CNFs-1 with isosurface of 0.61 e/Å3 (charge accumulation shown as cyan region). **f, g** ELF of the molecular structure of CNFs and CNFs-1. **h** Carrier mobility of the molecular structure of CNFs and CNFs-1 (the carrier type is electron-hole).

"Supplementary Fig. 7a presents a schematic diagram of the electronic band structure of cellulose triboelectric materials. The triboelectric charge generated by contact electrification is retained in the carrier traps of the band structure of the triboelectric material. The energy barrier and capture cross-section of the carrier traps confine the triboelectric charge to the electronic bandgap structure of the material. Density functional theory (DFT) analysis of the density of states (DOS) of CNFs films and the sensing material CNFs-1 reveals (Supplementary Fig. 7b, c) that the bandgap of CNFs films is only 0.75 eV, indicating that the carrier traps in the bandgap of CNFs films are closer to the band edges, requiring lower energy and resulting in weaker charge retention capability. The bandgap of CNFs-1 is significantly increased to 1.61 eV, and the bandgap of the triboelectric material in the charge retention phase is as high as 1.61 eV. The carrier traps for triboelectric charge are located far from the conduction band minimum and valence band maximum, respectively, which can better retain triboelectric charge and improve the sensor response signal.

To further investigate the redistribution of electrons in the molecular structure, the electron localization function (ELF) was calculated and topological analysis was performed. Supplementary Fig. 7d, e show the three-dimensional ELF visualization maps with an isosurface value of 0.61 e/Å3, respectively. The blue regions in the figures represent the electron distribution areas. Compared with CNFs, CNFs-1 has more blue distributions, indicating more electron distributions. The two-dimensional quantitative ELF images (Supplementary Fig. 7f, g) also show that the molecular structure of CNFs-1 has more electrons around it, indicating that in the charge retention phase, the transport process of triboelectric charge (carriers) makes it easier for triboelectric charge to bind with carrier traps, significantly improving triboelectric charge retention, which is more conducive to a higher sensor response signal in high-temperature environments.

To analyze the motion state of the charge in the sensing material, the carrier mobility is studied based on the variable situation theory proposed by Bardeen and Shockley, as shown in the equation:

$$\mu = \frac{eh^3 C}{K_B T m^* m_d E_1^2}$$

Where e represents the elementary charge, $\hbar$ represents Planck's constant divided by 2π, K_B represents the Boltzmann constant, T represents the temperature set at 300 K. m* denotes the effective mass of electrons or holes, and the carrier mobility can be derived from the derivative of the electronic band structure using the following formula, as illustrated in Supplementary Fig. 7h. The results reveal that the CNFs film molecular structure exhibits a high carrier mobility (24298 $cm^2V^{-1}s^{-1}$), indicating the rapid motion of retained triboelectric charges within the band structure. Compared to CNFs, CNFs-1 exhibits further enhanced carrier mobility (46500 $cm^2V^{-1}s^{-1}$). DOS and ELF analyses demonstrate that CNFs-1 possesses a high triboelectric charge retention capability, leading to a more pronounced electrical response to stimuli. Additionally, CNFs-1 exhibits faster triboelectric charge motion. Under elevated temperatures, the rapidly moving triboelectric charges are susceptible to hot electron emission, resulting in a faster temperature change response for CNFs-1 in high-temperature environments."

Furthermore, it is crucial to clarify that our research extends beyond merely reporting on high-temperature material design and heat-resistant pressure sensors. Inspired by the Sahara silver ant and biological sensing mechanisms, we have biomimetically developed a novel approach for achieving dual-response to both temperature and pressure in extreme environments (Fig. 1). This innovative method represents the advancement in the field of environmental sensing under harsh conditions. We appreciate your valuable feedback once again.

[REDACTED]

Fig. 1 | Schematic illustration of the bioinspired triboelectric sensor. a Nervous system of the Saharan silver ant for bimodal signals of pressure and temperature under high temperatures. **b** Signals perceived by the triboelectric sensor for machine learning to identify objects.

6. The T-TENG in the manuscript essentially operates as a single-electrode device, which is subject to severe electromagnetic interference, making it difficult to distinguish valid signals from interference in practical applications.

Response: We sincerely appreciate your profound insights regarding the electromagnetic interference challenges faced by our T-TENG device. Your observations keenly highlight a critical issue pertaining to single-electrode triboelectric nanogenerators. We have carefully considered your feedback and respond as follows.

(1) As mentioned by the reviewer, electromagnetic interference (EMI) during the operation of the T-TENG in practical applications is indeed unavoidable. EMI can lead to signal distortion, making it difficult to extract effective signals from background noise (ACS Appl. Mater. Interfaces, 2022, 14(35): 40014-40020). Therefore, we closely analyzed the signal-to-noise ratio (SNR) of the T-TENG in realistic scenarios, with equipment such as electrometers, linear motors, and heating plates in the vicinity during our experiments. The results demonstrated that our T-TENG device exhibits excellent signal sensing capability at various temperatures: a. The peak intensity of the effective signal generated by the T-TENG is at least an order of magnitude higher than the background electromagnetic interference (Fig. R2), indicating a high SNR. This significant difference in signal intensity provides a solid foundation for subsequent

signal processing and feature extraction; b. By employing machine learning algorithms to classify the acquired signals, we achieved a 94% accuracy rate in effective signal recognition, further validating the T-TENG's capability to distinguish between effective signals and interference.

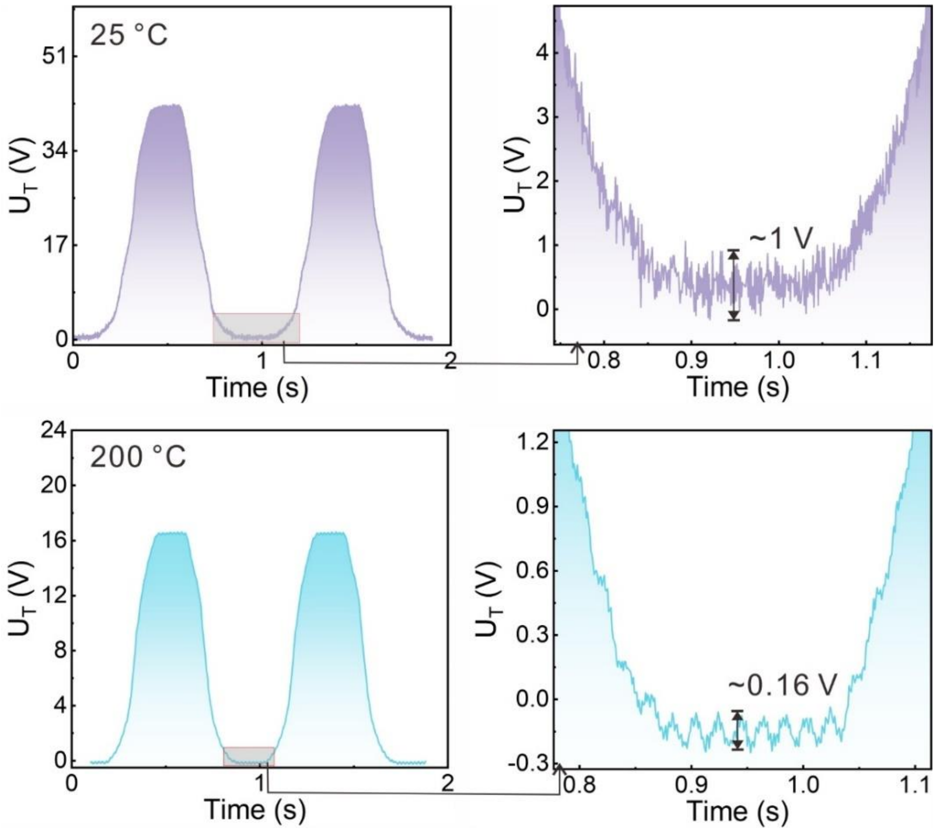

Fig. R2 | Interference effects of T-TENG at different temperatures.

(2) When the signal output is insufficiently large, crosstalk presents a significant challenge for TENG-based sensing devices and arrays (Nano Energy, 2021, 81: 105590). To enhance the intrinsic anti-interference capability of the T-TENG, we implemented measures in material design, structural construction, and circuit design. Firstly, the cellulose materials were chemically modified. Our studies indicate that this method improves the carrier retention rate, thereby effectively preventing charge dissipation (Supplementary Fig. 7), which enhances the anti-interference potential to some extent. Secondly, following previous research (Adv. Funct. Mater. 2018, 28, 1802989; Mater. Today 2018, 21, 216-222), we applied a grounded, highly conductive shielding silver film on the surface of the T-TENG, which acts as a Faraday cage to minimize undesirable components in the output signal due to inadvertent touches or changes in working conditions, such as touching different objects with wet or dirty fingers, thereby shielding electrostatic interference and improving device reproducibility. Finally, a common issue with single-electrode triboelectric sensor arrays is the contradiction between multiplex design and severe misidentification, primarily due to electrical signal interference between sensing nodes and internal

circuits (Nat. Commun. 2024, 15, 1238). This issue arises from complex, high-density electrode wiring designs during multiplexing and large-area detection. High-density wiring inherently generates substantial electrical signals due to triboelectric and electrostatic induction when subjected to external force/touch, making it challenging to accurately recognize real signals triggered by sensing pixels. Thus, we learned from systematic previous studies by treating each T-TENG sensor as a tactile sensing unit, connecting each unit with serpentine metal wiring for data collection (Nano Energy 2021, 81, 105590), and maintaining a height difference between the sensor units and electrodes (Microsyst. Nanoeng. 2020, 6, 59) to suppress interference.

(3) Significant research progress has also been made in using single-electrode TENGs for practical sensing applications (Adv. Mater. 2022, 34, 2203073). Researchers have made extensive efforts to tackle the issue of signal vulnerability to EMI in single-electrode mode sensor arrays, such as establishing a precise configuration of sensing nodes and electrodes (Nano Energy 2018, 50, 497-503). Moreover, some recent excellent studies have adopted direct current triboelectric generators based on the principles of contact electrification and electrostatic breakdown to reduce circuit use (Nat. Commun. 2020, 11, 6186; Nat. Commun. 2021, 12, 4686), and combined them with optical signals (Energy Environ. Sci. 2023, 16, 4641-4649) to shield EMI, providing more solutions for the extensive application of TENGs.

7. Experiments and all data are carried out and obtained in ideal experimental environments under standard conditions, and there is a lack of practical application demonstrations (e.g., videos) reflecting the core functionality of the dual-fusion sensor. Meanwhile, except for the temperature, other factors, like moisture, light and etc. would also affect the surface charge, so the output signal would be complicated in the real situation.

Response: Thank you for your insightful comments on our manuscript. We greatly appreciate your feedback and the opportunity to address the issues you raised. We acknowledge that the initial experiments were conducted under controlled laboratory conditions to establish the basic principles and performance of our dual-modal sensor. However, we recognize the importance of demonstrating real-world applications. In response to your valuable suggestions, we have conducted additional experiments in various real-world settings and prepared a video demonstration (Supplementary Movies 2, 3) that showcases the core functionalities of the sensor in these environments. These contents have been included in the revised manuscript and supplementary information.

Additionally, in our application tests, we used only symmetrical objects to evaluate the system's performance. To increase the complexity of the application for object recognition, we expanded the dataset to include asymmetrical objects and retrained our neural network. The results indicate that our system demonstrates excellent recognition performance with an average accuracy of 94%. Furthermore, as a proof of concept, we extended the application of the sensing system to not only recognize the type of objects but also to identify their temperature, this enhanced capability covering both symmetrical and asymmetrical objects. These additional experiments further validated the effectiveness and versatility of our sensing system, and we believe these new results have improved our manuscript.

Regarding the impact of other environmental factors on surface charge, we agree that humidity, lighting, and other variables indeed affect the sensor's output. To address this issue, we conducted electrical signal response tests under humid environments and high-intensity UV light conditions, quantifying the impact of these factors on our sensor's performance to ensure reliable sensing data even in complex situations. The stability of the sensing signal in high humidity and strong UV illumination environments is maintained thanks to the stability of the material and the encapsulation of the shell and electrodes. The detailed results and discussions of these experiments will be added to the manuscript. Thank you again for your constructive feedback, which has helped us improve the quality and relevance of the research. The specific revisions to the manuscript content are as follows.

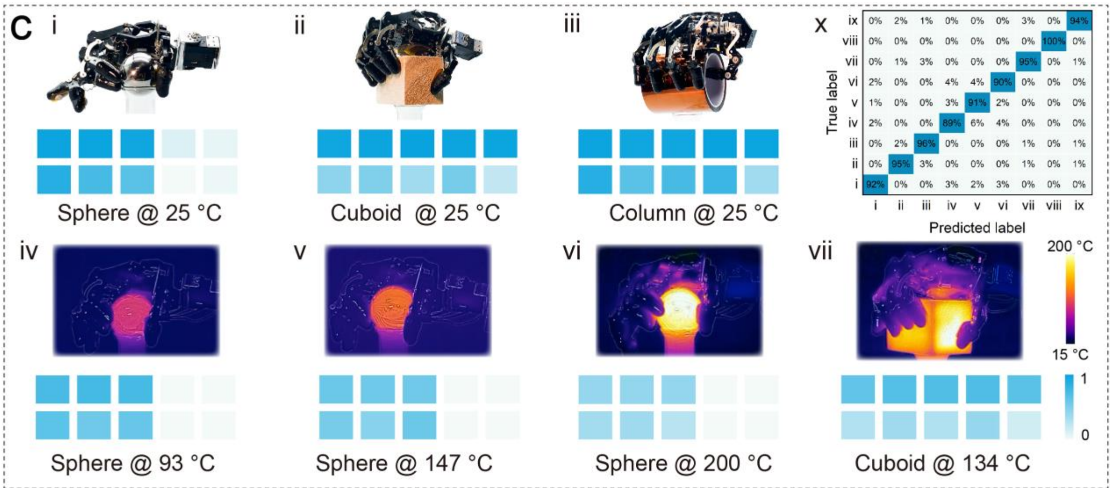

Fig. 6 | Tactile perception in high-temperature environments. c Robot hand with integrated triboelectric sensors for object shape and temperature recognition in complex environments.

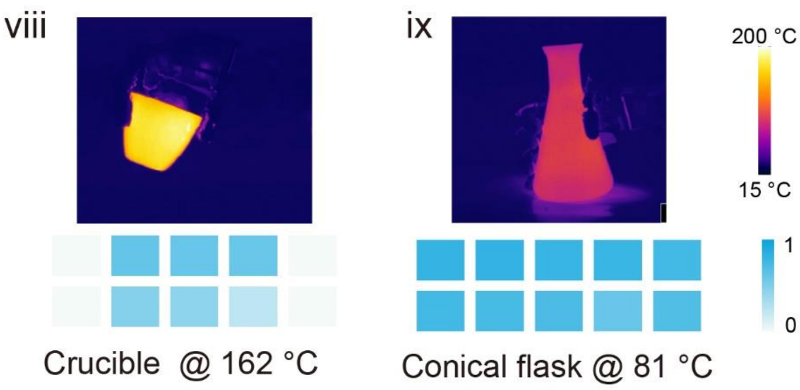

Supplementary Fig. 15 | The recognition of asymmetric objects.

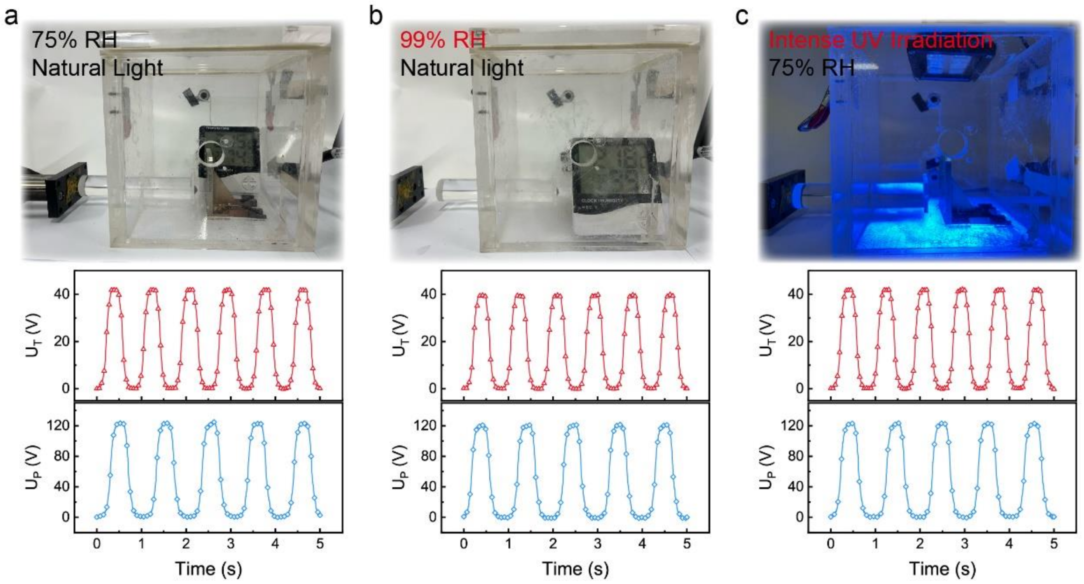

Supplementary Fig. 14 | The electrical signals under humidity and UV light.

Finally, we thank the reviewer again for these thoughtful comments. The manuscript has greatly benefited from these insightful suggestions. We greatly appreciate the valuable opportunity provided by the reviewers to illustrate the importance of this research and sincerely hope that our response will address the reviewer's concerns.

<u>Reviewer #3 (Remarks to the Author):</u>

The manuscript reports tactile sensor based on triboelectric generator. The sensor is capable of working at high temperature (200 deg celsius) and able to recognise objects of different shapes. The sensor has fast response and recovery time. The manuscript lacks sufficient details required to reproduced the methods. Further, the results are not supported by explanations. I want to reject the manuscript and following comments can be considered:

Response: We are deeply grateful to the reviewers for their meticulous review of our work and their insightful comments. We are pleased to accept and implement these suggestions to enhance the quality of our manuscript. Your feedback has prompted us to critically re-examine our study and identify key questions for improvement, leading to a more comprehensive and detailed manuscript. We recognize the need to provide more detailed information to facilitate reproducibility. To address your concerns, we have expanded the methods section, supplementing the manuscript with detailed information essential for replication, including the materials used in our research, the device fabrication process, and a comprehensive description of our testing procedures. We have provided specific descriptions and experimental tests for frequency, response time, and asymmetric object recognition, along with clarifications and revisions to ambiguous concepts and theoretical content within the manuscript. Importantly, we recognize the significance of meticulous, rigorous, and professional communication and sincerely apologize for any previous inaccuracies. We have revised the specific details of the COMSOL simulations and meticulously addressed numbering, grammatical, and other details throughout the manuscript.

We hope that our responses will address your concerns, and the revisions have been highlighted in red in the manuscript. Thanks again to the reviewers. Below is our point-by-point response to the comments.

1. The thickness of FEP and CNF is considered same in the COMSOL simulation which is not true. Further is it possible to consider surface roughness of nm range in the COMSOL simulations. If not, what is the reliability of simulation.

Response: We highly appreciate the reviewer's instructive suggestion, and we are very sorry for the improper data presentation and errors.

(1) As mentioned by the reviewers, thickness has a significant impact on the simulation results in COMSOL. In accordance with the suggestions, we have rigorously adjusted the thickness settings to reflect the actual dimensions used in testing, specifically the thickness of FEP to 50 μm and that of CNFs-2 to 63 μm. We have also revised the experimental section of the manuscript, incorporating more accurate material parameters to simulate the surface potential variations of the triboelectric sensor. These results are presented in both images and videos (Supplementary Fig. 8, Supplementary Movie 1) to better demonstrate the sensing mechanism. The detailed description is as follows.

"The COMSOL Multiphysics software was used to study the electric potential distribution of the triboelectric materials during contact electrification, with the thicknesses of FEP and CNFs-2 set at 50 μm and 63 μm, respectively."

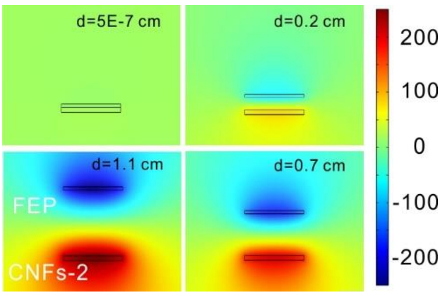

Supplementary Fig. 8 | Finite element simulation of surface potential variation of triboelectric materials.

(2) Based on the reviewers' expert opinions, we have recognized the lack of rigor in our parameter settings, and we sincerely apologize for this oversight. In our initial setup, we did not strictly adhere to the intrinsic properties of the materials; instead, we erroneously utilized centimeter-level parameters (with both materials having lengths

and widths of 9.6 × 1.6 cm, a semicircle radius of 0.8 cm, and a maximum separation distance of 10 cm). We are in full gratitude for your comments as they really alarm us to be serious to our work and prompt us to enrich our professional knowledge. The original intent behind simulating rough surfaces was to illustrate that, due to the applied force, more effective contact with rough surfaces would lead to increased surface charge generation, thereby enhancing the electrical signal output (Nano Energy 2016, 20, 283-293). We have removed the erroneous content and hope to gain your approval. Once again, we sincerely apologize for our mistakes.

2. What is the frequency used for response and recovery time. Is there any influence of frequency on the response and recovery time of the pressure sensor.

Response: We highly thank the reviewer's responsible suggestions for a better future readability. We sincerely apologize for this negligent experimental investigation and thank the reviewers for their meticulous review.

(1) In our study, a standard frequency of 2 Hz was used to measure the response and recovery time of the pressure sensor. This frequency was chosen based on the conditions of 1-3 Hz, which are common usage scenarios in the field of pressure sensors, and allows for comparison with similar studies. Specific experimental details have been added to the revised draft. The detailed description is following.

"When pressure was applied to P-TENG at 2 Hz, the response times to stress compression and recovery were 70 ms and 58 ms, respectively (Fig. 3e), and the higher response time is maintained at different frequencies (Supplementary Fig. 10), much faster than the human response time to tactile stimuli (139 ms)."

(2) To clearly illustrate the specific effects of frequency on the response and recovery times of the pressure sensor, five frequencies (3 Hz, 2.5 Hz, 2 Hz, 1.5 Hz, and 1 Hz) were investigated (Supplementary Fig. 10 and Table R2). In fact, frequency has a significant impact on the sensor's response and recovery times. The response time is determined by the contact and separation duration between the CNFs material and the FEP material during pressure sensing. Higher frequencies can significantly enhance the sensor's signal response and recovery times. Under rapid contact conditions at 3 Hz, the response and recovery times can be as fast as 37 ms and 42 ms, respectively. In contrast, under slower contact conditions at 1 Hz, both the response and recovery times can be maintained within 135 ms. Accordingly, we have revised the manuscript to clarify the descriptions related to response and recovery times. The detailed description is as follows.

"When pressure was applied to P-TENG at 2 Hz, the response times to stress compression and recovery were 70 ms and 58 ms, respectively (Fig. 3e), and the higher response time is maintained at different frequencies (Supplementary Fig. 10), much faster than the human response time to tactile stimuli (139 ms)."

Table R2 | Response and recovery times of the pressure sensor at 3 Hz, 2.5 Hz, 2 Hz, 1.5 Hz and 1 Hz.

Frequency	3 Hz	2.5 Hz	2 Hz	1.5 Hz	1 Hz
Response time (ms)	37	50	70	104	134
Recovery time (ms)	42	52	58	96	131

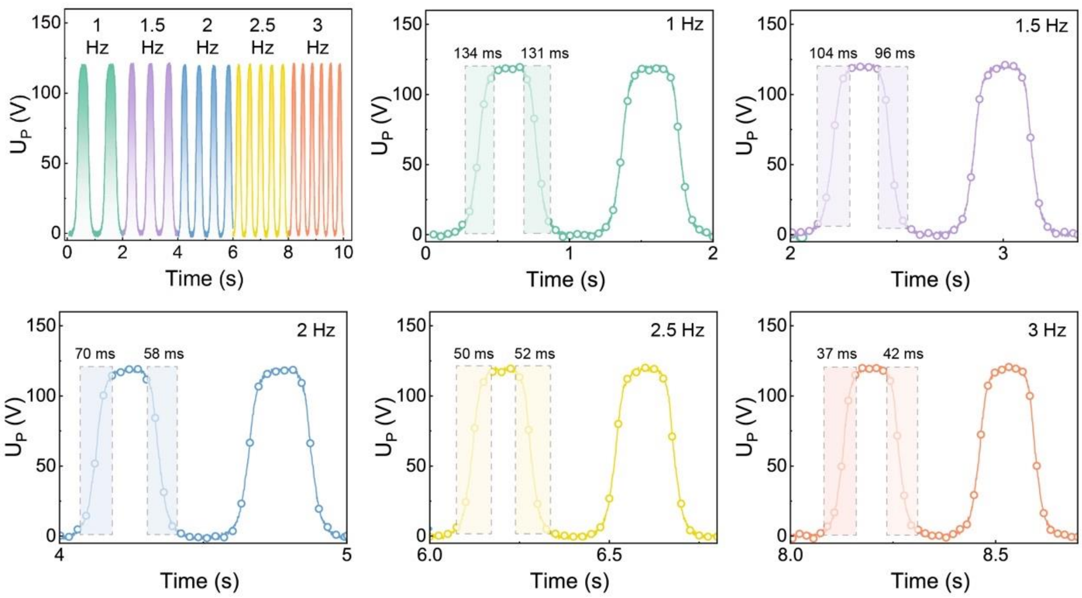

Supplementary Fig. 10 | Electrical signal and response time of the pressure sensor at 3 Hz, 2.5 Hz, 2 Hz, 1.5 Hz and 1 Hz.

3. Why frequency has no influence on the signal of pressure sensor?

Response: We thank the reviewer for their professional questions, and we apologize for the lack of sufficient explanations. The insignificant impact of frequency on the pressure sensing signal can be primarily attributed to the voltage signal response mechanism of the TENG. In an open-circuit state, there is no dynamic charge transfer process; consequently, the voltage signal solely depends on the electric potential difference between the positive triboelectric material (CNFs film) and the negative triboelectric material (FEP film). Throughout this process, variations in frequency do not significantly affect the voltage signal of the pressure sensor. In this context, our intention was to convey that the magnitude of the voltage signal serves as an intuitive representation for the pressure sensor. To enhance the article's readability, we have provided a more accurate description of the original text. Furthermore, we have supplemented the revised manuscript with a detailed theoretical analysis. The corresponding modifications are presented as follows.

"Supplementary Note 1 | Principle of triboelectric signal generation

According to the working principle of a TENG, when two triboelectric layers come into contact, due to the contact electrification effect, the inner surfaces of the two layers acquire opposing static charges of equal density σ (triboelectric charge Q). As the two layers begin to separate and distance x increases, a potential difference (V) is induced between the electrodes. Niu et al. (Nano Energy, 2015, 14: 161-192) studied the fundamental equations for contact-mode TENG, which can be used to calculate its output characteristics:

$$V = -\frac{Q}{S\varepsilon_0}\left(d_0 + x(t)\right) + \frac{\sigma x(t)}{\varepsilon_0}$$

Under open-circuit conditions, no charge is transferred, which means Q is 0. Thus, the open-circuit voltage V_{OC} can be expressed with the following Equation:

$$V_{OC} = \frac{\sigma x(t)}{\varepsilon_0}$$

Where σ is the triboelectric charge density, ε_0 is the vacuum permittivity, and x(t) is the gap between the two contact materials. From Equation, it is evident that during this process, the open-circuit voltage is independent of frequency and only increases with the rise in displacement. When the displacement x reaches x_{max}, the maximum open-circuit voltage is achieved (Nano Energy, 2019, 61: 111-118)."

4. Please include at least six data points to confirm the linear relationship for the sensors.

Response: Thank you for your insightful comments and valuable feedback on our manuscript. We greatly appreciate your suggestion to include additional data points to confirm the linear relationship for the sensors.

According to your suggestions, we re-evaluated the experimental setup and conducted additional tests to collect more data points. The revised manuscript now includes seven data points for the sensor, further confirming the linear relationships discussed previously. We believe that these enhanced data provide more evidence and clarity to our findings compared to the earlier version. We hope that these improvements meet your expectations, and we are sincerely grateful for your constructive guidance. The specific modifications are as follows.

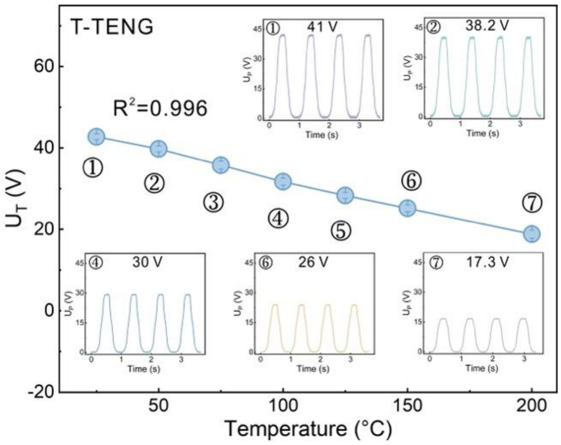

Fig. 3 | Temperature sensing. c Temperature sensing data.

5. "In the test at room temperature, the pressure response signal is unaffected by the temperature when the pressure exceeds 20 kPa". The reason for this is unclear.

Response: We greatly appreciate the reviewer's valuable suggestions, and we apologize for the difficulty in understanding the reviewers due to the wrong descriptions in the manuscript. The original meaning of this statement is that, during tests conducted at room temperature, the response signal of the T-TENG is unaffected by pressure when it exceeds 20 kPa. In the manuscript, "pressure" was incorrectly written as "temperature," and this error has been corrected in the revised version. As indicated by the theoretical analysis (Supplementary Note 3), the response signal is attributed to changes in contact area. The sensing materials of the T-TENG and P-TENG exhibit different surface structure designs (Supplementary Figs. 5, 6). The sensing material of the T-TENG (CNFs-1 film) has a smooth surface, allowing it to reach saturation pressure quickly and remain unchanged over a broader pressure range, only responding to variations in temperature. Therefore, when the pressure exceeds 20 kPa, the response signal of the T-TENG is not influenced by pressure. We appreciate your attention to this critical detail, and we have made the necessary revisions and additions to the main text. The modifications are as follows.

"Notably, the T-TENG exhibits pressure insensitivity in temperature sensing (Fig. 4d). This is due to the smooth surface and constant contact area, making the pressure value quickly reach equilibrium"

"**Supplementary Note 2 |** Theoretical analysis of pressure and voltage sensing signal (J. Mater. Chem. A, 2021, 9(36): 20100-20130)

Usually, under pressure P, the output voltage V_p of a TENG equals the open-circuit voltage V_{OC} in that state, which can be expressed by formula:

$$V_p = \frac{\sigma_0 d_p}{\varepsilon_0}$$

Where ε_0 is the vacuum permittivity constant, and σ_0 is the triboelectric charge density, considered constant. Assume the initial gap distance is d_0 with a change Δd, and d_p is the distance under pressure P. The gap distance and open-circuit voltage under pressure P can be calculated as follows:

$$d_p = d_0 - \frac{d_0}{Y} P$$

$$V_p = \frac{\sigma_0}{\varepsilon_0}\left(d_0 - \frac{d_0}{Y} P\right)$$

Where Young's modulus Y, the initial distance of the gap layer d_0, triboelectric charge density σ_0 , and permittivity constant ε_0 can be considered constants. The open-circuit voltage V_p is expected to have a direct linear relationship with the external pressure P, making it a reliable parameter for measuring the pressure applied to the sensor. The sensitivity calculation equation for the triboelectric pressure sensor is as follows:

$$S = d(\Delta V/V_s)/dP,$$

Where ΔV is the relative change in output voltage, and V_s is the minimum detectable electrical signal. Different voltage increases lead to different sensitivities. Hence, the larger the voltage signal, the higher the sensitivity (Adv. Mater., 2022, 34(29): 2203073; Adv. Funct. Mater., 2019, 29(41): 1806379)."

6. What is the sensitivity, response and recovery time of the temperature sensor.

Response: We thank the reviewer for their professional questions, and we apologize for the lack of sufficient experimental results and explanations. The performance testing experiments of the temperature sensor have been supplemented. At an operating frequency of 2 Hz, the sensitivity is measured at 0.14 V $°C^{-1}$, with a response time of 67 ms and a recovery time of 63 ms. This information has been included in the revised manuscript, specifically described as follows.

Note R1 | T-TENG sensitivity calculation equation：

$$S = \frac{d(\Delta V/V_s)}{dT}$$

Where ΔV is the relative change of the output voltage, Vs is the minimum detectable electrical signal, T is the changing temperature.

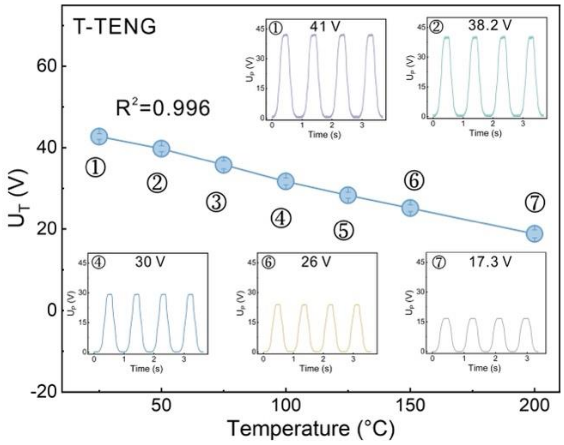

Fig. 3 | Temperature sensing. c Temperature sensing data.

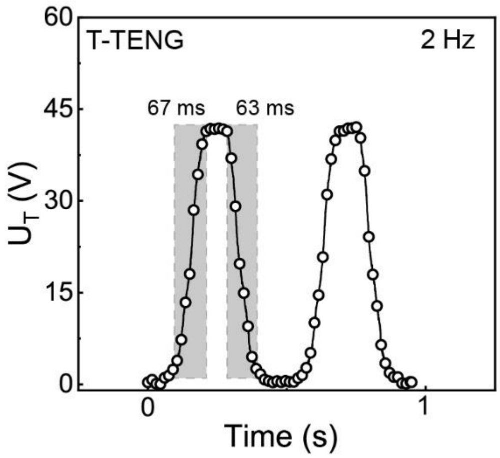

Supplementary Fig. 11 | Response and recovery time of T-TENG.

7. The experimental section is unclear and doesn't provide enough details on the methods used. It is not clear how the temperature measurements were performed.

Response: Thank you for your valuable feedback. We apologize for the lack of clarity in the experimental section and appreciate your guidance in improving this aspect of our manuscript. We have revised the section to include a comprehensive explanation of the methodologies employed. Specifically, we have detailed the temperature measurement process, including the equipment used and the calibration procedures performed to ensure accuracy. We hope this will solve your doubts, but please let us know if further modifications are needed. We are grateful for your constructive comments, which have significantly enhanced the quality of our work. We made More detailed descriptions have added in the revised manuscript, and the specific modifications are as follows.

"The electrical performance of the dual TENGs was measured using a Keithley 6514 electrometer. For standard measurement of electrical output, a commercial linear mechanical motor is used to apply a constant contact force, with the magnitude of the applied force measured by a HYPX-601 instrument. The prepared T-TENG and P-

TENG are respectively attached to the fixed side of the motor, and pressure is applied to the devices using a linear motor. The generated electrical signals are measured by the electrometer, then collected by a data acquisition card, and the final data is transferred to computer software for display. A schematic diagram of the experimental setup is shown in Supplementary Fig. 16."

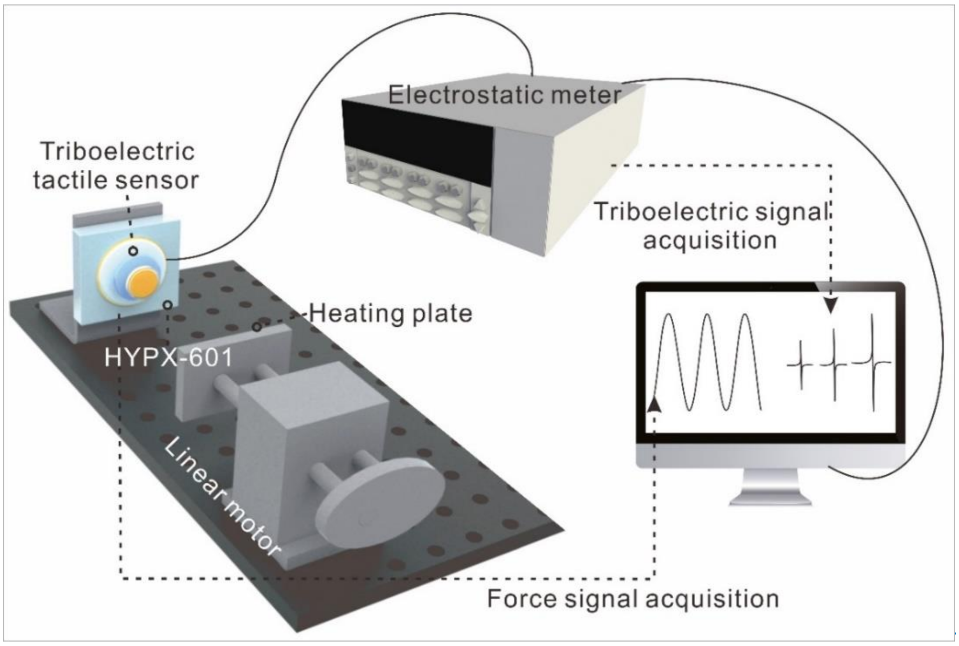

Supplementary Fig. 16 | Diagram of the electrical performance testing device.

"Preparation of triboelectric materials

High-purity cellulose material was obtained by purifying bagasse pulpboard and then transformed into nanoscale size by high-pressure homogenization. With a slurry concentration of 1%, the dry weight of the sample was determined to be 0.4 g. The CNFs film material (thickness 62 ± 4 μm) was prepared by vacuum-assisted fibril self-assembly followed by hot pressing and drying. Then, the CNFs film was treated by low-temperature plasma technology, with oxygen as the discharge gas, at a power of 100 W for 10 min, to obtain a CNFs film with micro-nano structures on the surface54. Subsequently, the CNFs film and a CNFs film with protruding structures were separately immersed in a 3 wt% APTES solution for 2 h, then sufficiently washed with ethanol and dried in an oven at 120 °C to obtain the final temperature sensing material CNFs-1 film and pressure sensing material CNFs-2 film. The detailed preparation process is shown in Supplementary Fig. 4a.

Preparation of triboelectric sensor

First, the CNFs-1 film with a diameter of 5 mm and coated with Ag on the back is adhered to the silicone shell (bottom diameter 10 mm, top diameter 5 mm) as the positive triboelectric material of the T-TENG. Subsequently, the FEP (thickness 50 ± 2 μm, diameter 7.5 mm), serving as the common negative triboelectric material for the multimodal sensor, is attached to the middle of the silicone shell. Finally, the circular CNFs-2 film with a diameter of 10 mm is attached to the bottom of the shell, and conductive copper wires are respectively attached to the backs of the CNFs-1 and CNFs-2 films, thus forming a single-electrode mode multimodal sensor. Lastly, the silver paint is sprayed onto the surface of the sensor.

Characterizations

The surface morphology of the material was analyzed by a scanning electron microscope (TESCAN MIRA LMS) and an atomic force microscope (BRUKER, USA). A Fourier transform infrared spectrometer (TENSOR II, BRUKER, Germany) was used to observe the chemical changes of the samples, and a simultaneous thermal analyzer (TG 209 F3 Tarsus, Germany) was used to test the thermodynamic behavior of the materials. The COMSOL Multiphysics software was used to study the electric potential distribution of the triboelectric materials during contact electrification, with the thicknesses of FEP and CNFs-2 set at 50 μm and 63 μm, respectively. An electrometer (Keithley 6514, USA) and a data acquisition card (NI-USB6259, USA) were used to record the electrical signals. Pressure, speed, and frequency were controlled by a linear motor (HYPX-601, China) equipped with a pressure sensor. A multichannel switch multimeter (Keithley DAQ6510, USA) was used to record multiple signals of the multimodal tactile sensor. Density Functional Theory (DFT) calculations were performed using the Vienna ab initio Simulation Package (VASP) combined with the projector augmented wave method. The Perdew-Burke-Ernzerhof (PBE) functional, following the generalized gradient approximation, was employed for the exchange-correlation functional. A $2 \times 2 \times 1$ K-point grid was used for sampling the Brillouin zone, and the energy cutoff was fixed at 500 eV. Structural relaxation continued until the convergence thresholds for energy and force were met at 1×10^{-4} eV and 0.03 eV $Å^{-1}$, respectively."

8. "The temperature dependent cross coupling error of P TENG is less than 0.4%". Please elaborate this.

Response: We greatly appreciate your insightful comments regarding the cross-coupling error of our triboelectric sensors. We are thankful for the opportunity to clarify this crucial aspect of our research.

Cross-coupling error refers to the unintended influence of one measured parameter (in this case, temperature) on the measurement of another parameter (pressure). Our objective was to develop a sensor with minimal cross-sensitivity between pressure and temperature sensing. In our study, we compared the experimental results (Fig. 5b) with theoretical predictions (Supplementary Fig. 12) to assess the cross-coupling error. The specific evaluation method involved comparing the deviation of each actual experimental data point from the theoretical prediction data, and calculating the average of the cross-coupling errors for all data points to obtain the final cross-coupling error.

For the pressure-sensing triboelectric nanogenerator (P-TENG), we found that the temperature-dependent cross-coupling error was less than 0.4%. This indicates that the impact of temperature variations on pressure signals is minimal, demonstrating that P-TENG can measure pressure with high accuracy and reliability across different temperatures. Similarly, for the temperature-sensing triboelectric nanogenerator (T-TENG), the pressure-dependent cross-coupling error was less than 3.2%. Although this value is slightly higher than that of P-TENG, it still represents a low level of cross-sensitivity, ensuring that pressure changes do not significantly affect temperature signals. These low cross-coupling errors (0.4% for P-TENG and 3.2% for T-TENG) demonstrate the effectiveness of our sensor design in minimizing cross-sensitivity between pressure and temperature sensing. The minimized interference is critical for ensuring the reliability and accuracy of our sensors. We hope this detailed explanation provides a clear understanding of our findings.

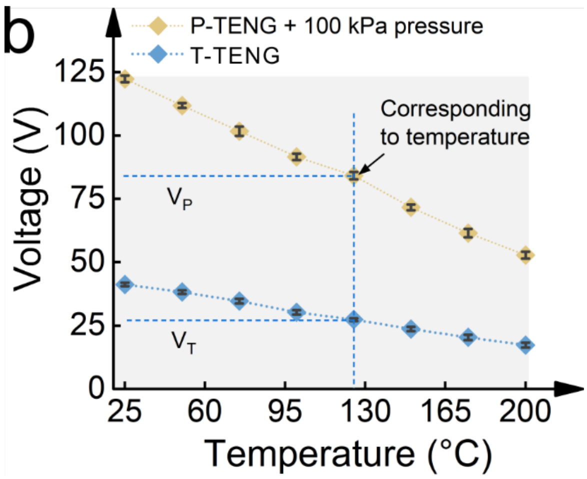

Fig. 5 | Pressure-temperature decoupling and dual-modal sensing in a single triboelectric sensor. b Response signals of P-TENG and T-TENG at different temperatures under the pressure of 100 kPa.

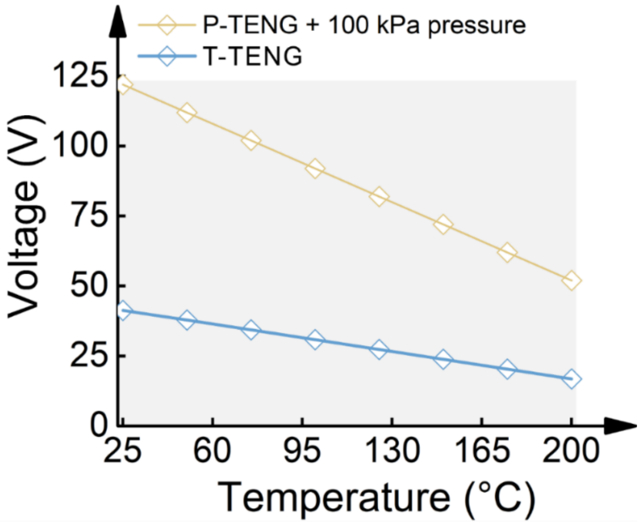

Supplementary Fig. 12 | The cross-coupling error of P-TENG and T-TENG under different temperatures at 100 kPa is less than 0.4% and 3.2% respectively compared with the actual test signal.

9. For fig. 4f what is the scenario when both temperature and pressure changes at same time.

Response: Thank you for your insightful comment regarding Fig. 4f. We appreciate your attention to detail and the opportunity to improve our manuscript. You raised an excellent point about the scenario where both temperature and pressure change simultaneously. We need to clarify an error in Fig. 4f (now Fig. 5f) here. The third condition change in Fig. 5f should be an increase in both pressure and temperature, with the temperature and pressure rising from 75 °C and 80 kPa to 150 °C and 100 kPa, respectively. To more clearly demonstrate this change, we have added a detailed diagram of the changes in pressure and temperature during the continuous variation (Supplementary Fig. 13). During the continuous variation, it can be seen that when both pressure and temperature increase, the pressure sensor P-TENG shows a rapid rise in response voltage due to the pressure impact, while the temperature sensor T-TENG is unaffected by the increase in pressure. Subsequently, both sensors are influenced by the temperature, and within a matter of seconds, the response voltage rapidly decreases to adapt to the appropriate temperature range and remains stable at 150 °C.

The revised Fig. 5f demonstrates how the system behaves when temperature and pressure are altered concurrently, providing a more comprehensive understanding of the phenomenon under study. We believe this addition significantly enhances the depth and breadth of our analysis, offering a more complete picture of the system's behavior under various conditions. We thank you for bringing this to our attention, as it has undoubtedly strengthened our research. We hope that this addition satisfactorily addresses your concern. Please let us know if you require any further clarification or have additional questions. The details are as follows.

[REDACTED]

Fig. 5 | Pressure-temperature decoupling and dual-modal sensing in a single triboelectric sensor. f Real-time response of the triboelectric sensor when subjected to temperature and pressure stimuli.

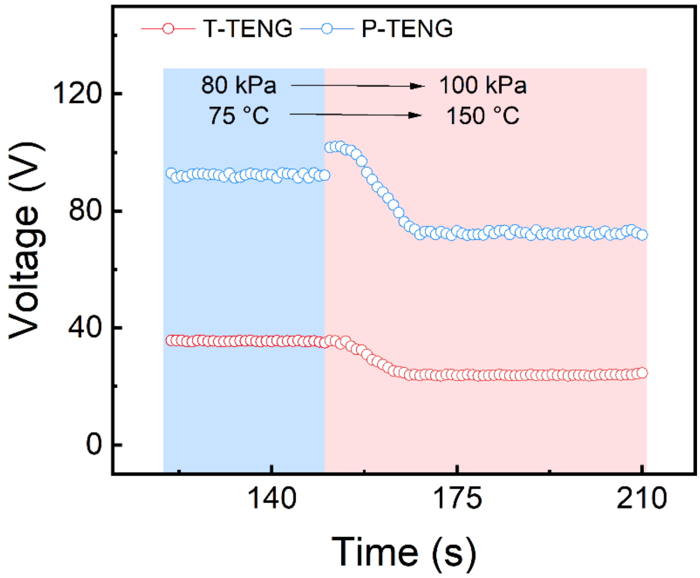

Supplementary Fig. 13 | The electrical signal in which pressure and temperature change simultaneously.

10. Please demonstrate identification of objects by including non-symmetric objects.

Response: Thank you for your constructive comment. To address your concern, we have performed additional experiments to demonstrate the identification of non-symmetric objects using our sensing system.

In our previous tests, we only evaluated the system's performance using symmetric objects. To fulfill your request, we have expanded our dataset to include non-symmetric objects and retrained our neural network. The results show that our system exhibits excellent identification performance, achieving an average accuracy of 94%. Additionally, as a proof of concept, we have extended the application of our sensing system beyond mere object type identification to include temperature detection. This enhanced capability applies to both symmetrical and asymmetrical objects. These additional experiments have further validated the effectiveness and versatility of our sensing system, and we hope that these revisions will solve your doubt.

"Fig. 6cviii shows the confusion matrix of the classification results of 9 objects, where each row represents a test sample in an actual category, and each column represents a predicted category. The results demonstrate that the system has excellent recognition performance for symmetric and asymmetric objects, with an average recognition accuracy of 94%. Furthermore, as a conceptual validation, the sensing system was used to identify the types and temperatures of objects."

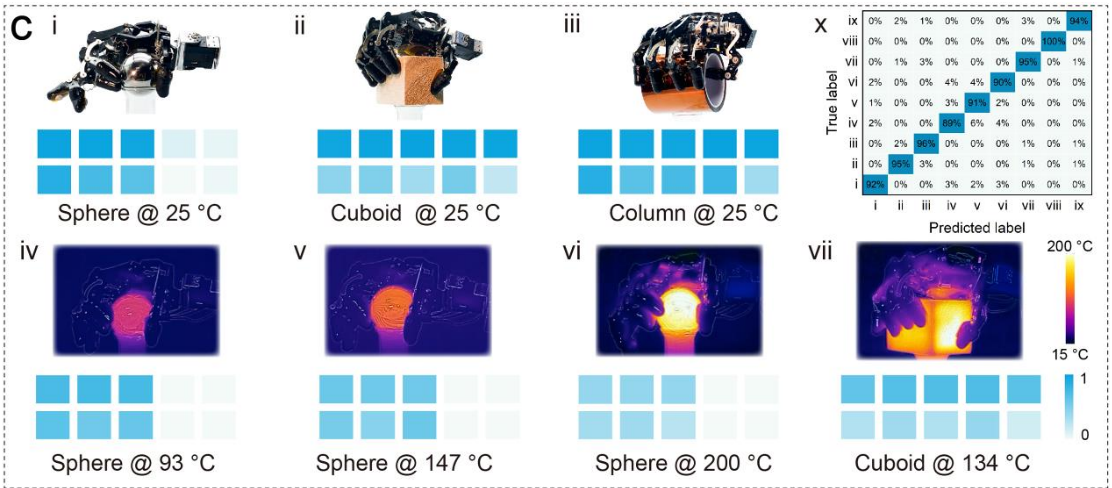

Fig. 6 | Tactile perception in high-temperature environments. c Robot hand with integrated triboelectric sensors for object shape and temperature recognition in complex environments.

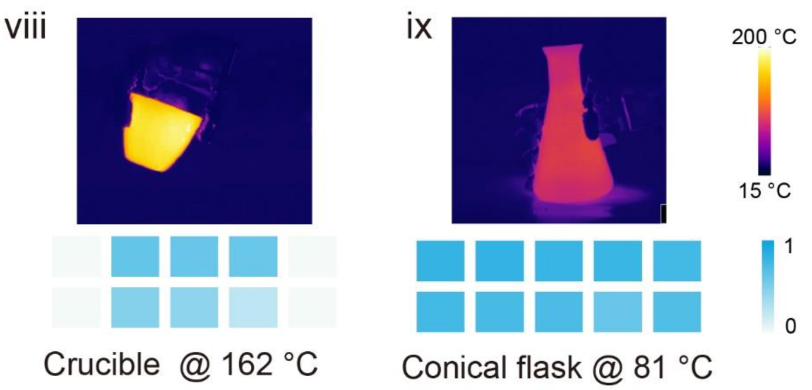

Supplementary Fig. 15 | The recognition of asymmetric objects.

11. The authors are advised to check throughly for the spelling and grammatical errors. Please also check figure numbers for example Line 150 includes figure 3f but its 2f.

Response: Thank you for your thorough review of our manuscript. We appreciate your attention to detail and apologize for any errors that may have been overlooked. We have carefully reviewed the manuscript and have corrected all spelling and grammatical errors. Additionally, we have double-checked the figure numbers and corrected the mistake in Line 150, where Fig. 3f was incorrectly referred to as Fig. 2f (A new drawing has been added to the revised manuscript, which is now expressed as Fig. 4f). Thank you for pointing out this error, and we are confident that the corrected manuscript is now free of such mistakes. We have made every effort to ensure the accuracy and clarity of our work.

Finally, we sincerely appreciate the thoughtful and insightful comments. The manuscript has greatly benefited from these comments.

Point-by-point Response to Reviewers' Comments

(Manuscript ID: NCOMMS-23-63750A-Z)

Reviewer #1 (Remarks to the Author):

Author addressed all the comments. It can be accepted for publication.

Response: We highly appreciate the reviewer for the professional opinions and suggestions, which have greatly helped us to improve the quality of our manuscript. We also appreciate your acknowledgment of our work and the acceptance of our manuscript in Nature Communications.

Reviewer #2 (Remarks to the Author):

Although the authors have spent efforts in revising the manuscript. The main concern is the novelty. I still don't think this work reaches the high standard level of Nature Communications.

Response: We sincerely thank the reviewer for carefully reviewing our work, and recognize our efforts in the revisions. We apologize for our insufficient description, which has left you concerned about the novelty of our work. We would like to provide further clarification to demonstrate the innovation and significance more comprehensively, and sincerely hope that our response will obtain your approval. The novelty of our work can primarily be summarized into the following five points:

1. Design Concept: Inspired by the Saharan silver ant and biological sensing mechanisms, we have developed a bionic approach to achieve dual-response sensing of temperature and pressure in extreme environments (Fig. 1), exploring alternative and complementary pathways for sensing in such conditions. This represents an advancement in the field of sensing under harsh conditions, different from traditional designs of high-temperature materials and pressure sensors, which is an area that has not been fully explored in existing literature.

2. Sensor Design: To address concerns about device novelty, we have added content about sensor material design and the latest research progress on triboelectric sensors in the revised manuscript.

(1) We appreciate the excellent literature references provided (Cellu 2019, 26, 5291-5303; Pet. Sci. 2023; Adv. Sci. 2020, 7, 2000258), which we have carefully read and analyzed. Compared to these published studies, our work demonstrates innovations in triboelectric sensing technology based on the intrinsic high-temperature resistance of cellulose, such as "investigating the ability of modified cellulose materials to reduce

carrier mobility through density functional theory; proposing and deeply exploring its charge retention capability and its preliminary dual-mode sensing under high-temperature conditions." These are research directions that have not yet been explored. To more intuitively show the differences, Table R1 summarizes the distinctions between the relevant references and this study.

(2) To fully demonstrate the differences of the CNFs material used in this study, we have detailed the preparation methods, chemical characteristics, and high-temperature resistance. The sensing materials (CNFs-1 and CNFs-2 films) were prepared based on high-temperature-resistant cellulose nanofibers, with detailed experimental procedures and characterization methods described in the supplementary information (Fig. S4).

(3) Furthermore, our work demonstrates the device's multi-sensory integration of temperature and pressure and investigates the underlying operating mechanisms, which may inspire the design of next-generation multi-responsive electronics for extreme environments.

3. Scientific Problems: The article described by the reviewer (Nat. Commun. 2015, 6, 8356) has greatly contributed to our work, for which we are deeply grateful. The dual-mode sensor in this study introduces a method based on the principle of triboelectric principles, which is expected to bring technological innovation to this field. Meanwhile,

o

u

r

4. Performance Focus: Zhang et al. (Nat. Commun. 2015, 6, 8356) achieved precise temperature resolution (<0.1 K) and high-pressure sensing sensitivity (28.9 kPa⁻¹), while our work achieved a signal output (20 V) over three orders of magnitude higher than related studies (0.3 mV), resulting in a good signal-to-noise ratio. The comparison table is shown in Table R2.

5. Application Demonstration: To address concerns about practical applications, we conducted additional experiments to demonstrate the sensor's performance under different humidity and lighting conditions (Fig. S14), as well as its capability in asymmetric object recognition. These enhancements, supplemented by experimental data and video demonstrations (Fig. S15), illustrate the sensor's versatility and practical application value. Therefore, our work can be considered an advancement in the comprehensive experimental demonstration of multi-sensory perception under harsh environments.

In summary, we have strictly followed the reviewers' suggestions, and make every effort to show the novelty of the work. In the revised manuscript, we have added elements in the material design for the sensor, including the latest research progress on triboelectric sensors, and clearly explained how our design pushes the development of current technology. The novelty of our work lies not only in the fabrication of the dual-

t

e

m

p

mode sensor but, more importantly, in demonstrating its potential for successful application as a dual-response building block for temperature and pressure in extreme environments, exploring the possibilities of sensing under such conditions.

Once again, we sincerely thank you for your comments and genuinely hope that our response will gain your support and address your concerns. The specific details are as follows:

[REDACTED]

Fig. 1 | Schematic illustration of the bioinspired triboelectric sensor. a Nervous system of the Saharan silver ant for bimodal signals of pressure and temperature under high temperatures. **b** Signals perceived by the triboelectric sensor for machine learning to identify objects.

Table R1. Systematic comparison between this study and Cellu 2019, 26, 5291-5303, Adv. Sci. 2020, 7, 2000258

Frequency	Cellulose 2019, 26, 5291-5303	Adv. Sci. 2020, 7, 2000258	This work
Scientific problems	High-temperature resistant cellulose nanofibers/polyvinyl alcohol hydrogels	Pressure sensor for normal operation in high temperature and harsh environment	Simultaneous sensing of pressure and temperature at high temperatures (200 ℃)

Sensing mode	No	Pressure	Pressure/Temperature
Sensitivity	No	4.4 kPa^{-1}	9.21 kPa^{-1}
Signal to Noise Ratio	No	Low	High

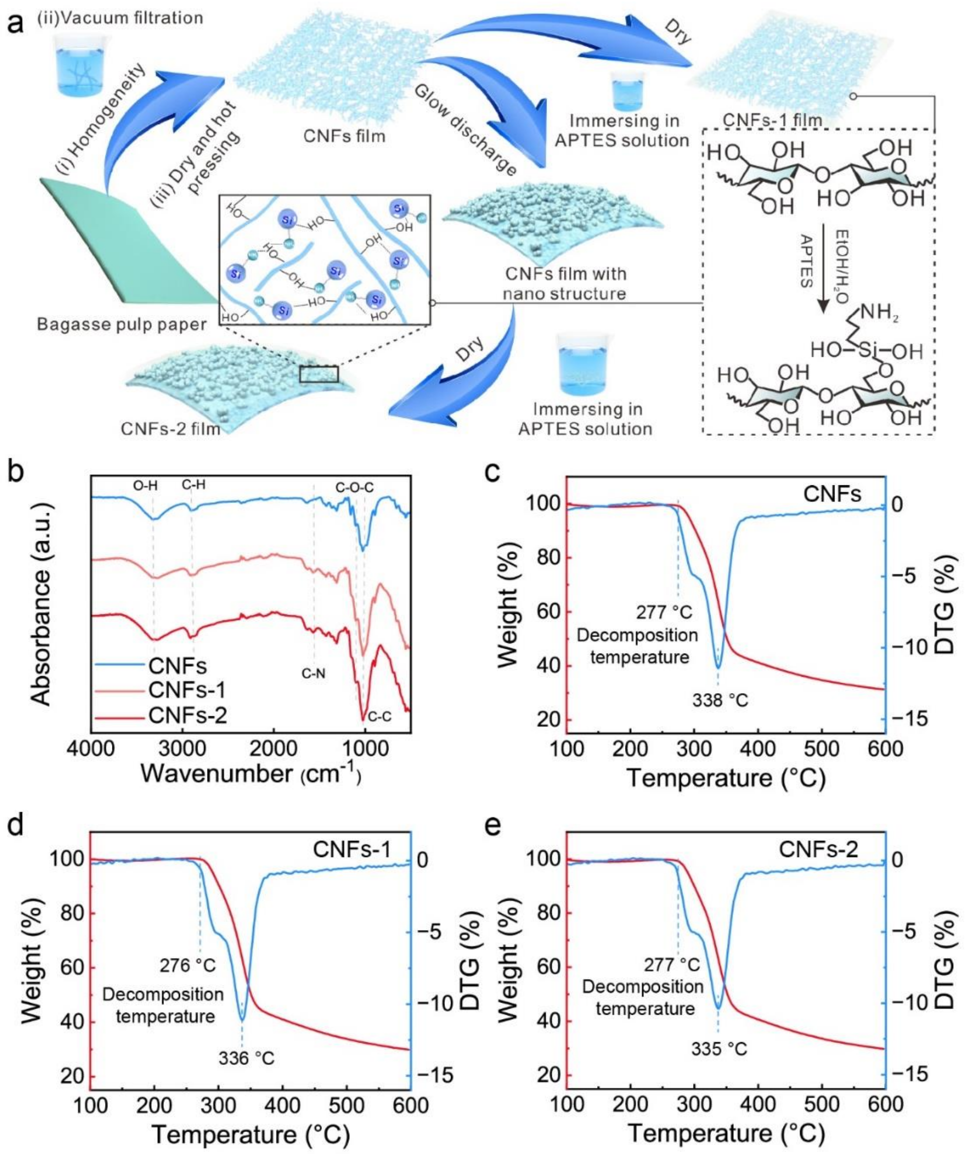

Supplementary Fig. 4 | Preparation of samples. a Schematic diagram of the preparation process of CNFs film, CNFs-1 film and CNFs-2 film (illustrated chemical process). **b** Fourier transform infrared spectral images of CNFs film, CNFs-1 film and

CNFs-2 film. **c-e** Thermogravimetric analysis images of CNFs films, CNFs-1 film and CNFs-2 film, respectively.

Supplementary Table 1 | Comparison of the temperature detection range of this work with reported multimodal sensors.

Multimodal sensing	Sensing mechanism	Temperature range (°C)	Reference
Pressure/temperature	Stress-optic/thermo-optic	26-35	*ACS Appl. Mater.*, 2023, 53264-53272
Pressure/temperature	Piezocapacitive/ thermoresistive	30-45	*Nat. Commun.* 2018, 9, 2458
Pressure/temperature	Piezo-tribophotonic/ thermoresistive	30-50	*ACS Nano* 2022, 16, 2789
Pressure/temperature	Reverse electrowetting/ thermogalvanic	5-31	*Angew. Chem. Int. Ed.* 2016, 55, 15864
Strain/temperature	Transmittance/ thermoresistive	25-42	*Small* 2023, 2301868
Pressure/temperature	Piezoresistive/thermoresistive	25-50	*Adv. Funct. Mater.* 2022, 32, 2107570
Strain/temperature /pressure	Mechanochromic/thermoresistive /triboelectric	0-50	*Adv. Funct. Mater.* 2022, 32, 2208362
Pressure/temperature	Triboelectric	25-200	This work

Table R2 | Systematic comparison between this study and Nat. Commun. 2015, 6, 8356

	Nat. Commun. 2015, 6, 8356	This study
Scientific problems	Sensitive temperature and pressure detection at the same time	Simultaneous sensing of pressure and temperature

		at high temperatures (200 ℃)
Monitoring temperature range	0-130 °C	0-200 °C
Sensitivity	28.9 kPa^{-1}	9.21 kPa^{-1}
Signal to Noise Ratio	Low	High

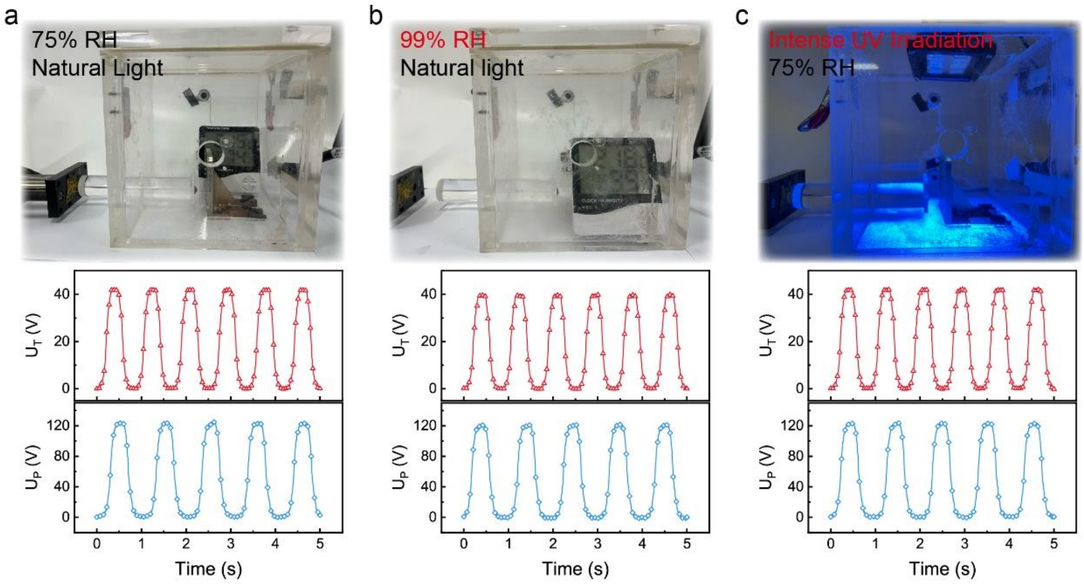

Supplementary Fig. 14 | The electrical signals under humidity and UV light.

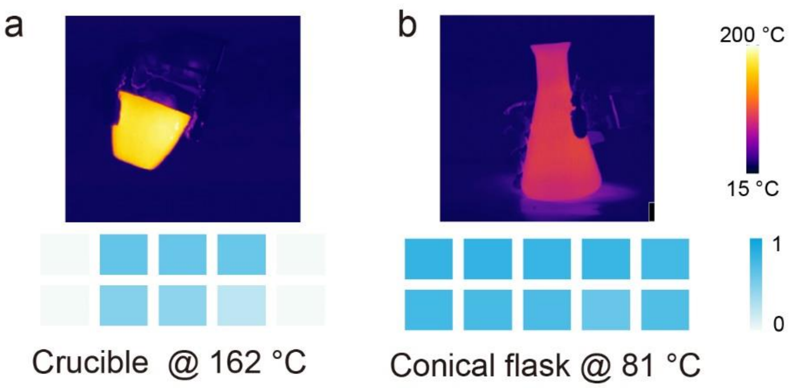

Supplementary Fig. 15 | The recognition of asymmetric objects.

Reviewer #3 (Remarks to the Author):

The raised comments are addressed well.

Response: We sincerely appreciate your valuable feedback on our manuscript. We also appreciate your recognition of our efforts in the revisions.

Reviewer #1 Version 0 Review Attachment:

A triboelectric tactile sensor beyond human touch perception

The proposed TENG design is unique and appreciate the authors for multimodal analysis with single device. The authors can modify their manuscript by inclusion of the following.

Review Comments:

1. How does the author confess that the CNF film have spherical bulge on it?
2. Figure 2 a and 2 b needs more explanation for easy understanding.
3. The author should include real time photographs of fabricated device. (With the surface and cross-sectional SEM image of CNF 2 to verify its spherical roughness)
4. How did the author perform electrical performance of the T-TENG and P-TENG? (Whether tested individually or multimodal setup itself)
5. Figure 3 d shows the pressure insensitivity of T-TENG, in a similar way does the P-TENG is temperature insensitive?